EMP Interaction With a Thin Cylinder Above
A Ground Plane Using the Singularity Expansion Method

by

T. H. Shumpert
Applied Research Group
The Dikewood Corporation
Albuquerque, New Mexico 87106

Abstract

The Singularity Expansion Method is employed to determine the transient response of a thin-wire scatterer arbitrarily oriented above an infinite perfectly conducting ground plane. An integro-differential equation is formulated for the current on the scatterer in terms of the complex frequency, $s = \sigma + j\omega$. The method of moments is used to reduce this integro-differential equation to a system of linear algebraic equations. The Singularity Expansion Method is then applied to determine the exterior natural resonances of the scatterer, the natural modes associated with these resonances, and finally the transient response of the scatterer to a unit step incident wave. The analytical and numerical techniques used to obtain the various terms in the singularity expansion representation of the transient response are discussed, and results are presented for several different orientations of the scatterer with respect to the ground plane.

PL 91-0942

Table of Contents

I. INTRODUCTION

The Singularity Expansion Method for the transient analysis of antenna and scattering problems was formalized and discussed in general by Baum [1]. Several other investigators [2], [3], [4] have also considered natural resonance techniques for conducting bodies. Analytical and numerical procedures for the determination of the transient response of a thin cylindrical scatterer using the Singularity Expansion Method have been developed and outlined by Tesche [5]. Similar techniques were used by Martinez, et al [6] to determine the transient response of a perfectly conducting sphere. Marin [7] has also applied this method to determine the natural resonances and transient response of a prolate spheroid. The numerical results obtained heretofore by application of the Singularity Expansion Method have demonstrated that this approach has several advantages over the classical approach (time harmonic analysis with Fourier inversion) for determining the transient response of conducting bodies isolated in free space.

The purpose of this note is to investigate these advantages for solving problems concerning the interaction between conducting bodies or between a conducting body and a ground plane. In particular, this note presents the transient analysis of a wire scatterer above a ground plane using the Singularity Expansion Method. A Pocklington type integro-differential equation is formulated for the current induced on a thin-wire scatterer above a ground plane in terms of the complex frequency, $s = \sigma + j\omega$. This integro-differential equation is reduced to a system of algebraic equations by the method of moments. Finally, the Singularity Expansion Method is applied to determine the transient response of the wire current to a unit step incident wave.

The exterior natural resonances and natural mode vectors are calculated and presented for various orientations of the scatterer with respect to the ground plane. The behavior of these quantities as

a function of the angle of inclination and height above the ground are plotted and tabulated for a wide range of these parameters. Typical time domain results for the current at several points on the scatterer are also included for several different wire orientations.

The results obtained using the singularity expansion method are compared with those given by Tesche [8] for the same geometry. These comparisons serve to correlate the data of the two studies and lend added confidence to the applicability of the Singularity Expansion Method to problems of this type.

II. FORMULATION

Consider the thin wire scatterer arbitrarily oriented above a perfectly conducting ground plane as shown in Figure 1. Note that the geometry as well as the parameters defining the geometry are identical with those in reference [8]. This greatly simplifies the comparison of the data of these two studies to be presented in a later section. As indicated in the figure, the total wire length is L, the distance from the center of the wire to the ground plane is h, and the angles ϕ and θ together determine the angle of inclination of the scatterer with respect to the ground plane. The geometry may be simplified by the introduction of a new angle, β, which represents the angle measured between the wire scatterer and its projection in the ground plane. Figure 2 shows the wire and its image in terms of the new angle β.

With the standard thin-wire approximations, one can write the expressions for the scattered vector and scalar potentials of the wire current and charge, $I_0(\xi)$ and $\rho_0(\xi)$, and the image current and charge, $I_1(\xi)$ and $\rho_1(\xi)$, as

$$\vec{A}_0^{\ s}(\xi) = \hat{\xi} \ \frac{\mu_0}{4\pi} \int_0^L I_0(\xi') \ G_0 \ (\xi, \xi') \ d\xi' \qquad (1)$$

5

$$\phi_o^S(\xi) = \frac{1}{4\pi\epsilon_o} \int_o^L \rho_o(\xi') \, G_o(\xi, \xi') \, d\xi' \qquad (2)$$

$$\vec{A}_1^S(\xi) = \hat{\zeta} \frac{\mu_o}{4\pi} \int_o^L I_1(\zeta') \, G_1(\xi, \zeta') \, d\zeta' \qquad (3)$$

$$\phi_1^S(\xi) = \frac{1}{4\pi\epsilon_o} \int_o^L \rho_1(\zeta') \, G_1(\xi, \zeta') \, d\zeta' \qquad (4)$$

where

$$G_o(\xi, \xi') = \frac{e^{-\gamma\left[(\xi-\xi')^2 + a^2\right]^{1/2}}}{\left[(\xi-\xi')^2 + a^2\right]^{1/2}} \qquad (5)$$

$$G_1(\xi, \zeta') = \frac{e^{-\gamma\left[\left(\left|L-\xi-\zeta'\right|\sin\beta - 2h\right)^2 + \left(\left|\xi-\zeta'\right|\cos\beta\right)^2\right]^{1/2}}}{\left[\left(\left|L-\xi-\zeta'\right|\sin\beta - 2h\right)^2 + \left(\left|\xi-\zeta'\right|\cos\beta\right)^2\right]^{1/2}} \qquad (6)$$

$$\beta = \frac{\pi}{2} - \arccos(\sin\theta\cos\phi) \qquad (7)$$

and

$$\gamma = \frac{s}{c}, \quad s = \sigma + j\omega, \quad c = \frac{1}{\sqrt{u_o\epsilon_o}} \qquad (8)$$

6

The ξ component of the scattered field at some point ξ on the surface of the scatterer is then given by

$$E_\xi^S (\xi) = - s A_\xi^S (\xi) - \frac{d}{d\xi} \phi^S (\xi) \qquad (9)$$

$$
\begin{aligned}
E_\xi^S (\xi) = &- \frac{\mu_o}{4\pi} s \int_o^L I_o (\xi, \xi') G_o (\xi, \xi') \, d\xi' \\
&- \frac{\mu_o}{4\pi} (\hat{\xi} \cdot \hat{\zeta}) s \int_o^L I_1 (\zeta') G_1 (\xi, \zeta') \, d\zeta' \\
&- \frac{1}{4\pi\epsilon_o} \frac{d}{d\xi} \int_o^L \rho_o (\xi') G_o (\xi, \xi') \, d\xi' \\
&- \frac{1}{4\pi\epsilon_o} \frac{d}{d\xi} \int_o^L \rho_1 (\zeta') G_1 (\xi, \zeta') \, d\zeta' \qquad (10)
\end{aligned}
$$

From the equation of continuity, we have

$$\frac{d}{d\xi} I_o (\xi) = - s \rho_o (\xi) \qquad (11)$$

$$\frac{d}{d\xi} I_1 (\zeta) = - s \rho_1 (\zeta) \qquad (12)$$

Using the foregoing relations, equation (10) may be written as

$$4\pi\epsilon_o s E_\xi^S (\xi) = \int_o^L I_o (\xi') \mathcal{L}_o G_o (\xi, \xi') + \int_o^L I_1 (\zeta') \mathcal{L}_1 G_1 (\xi, \zeta') \, d\zeta'$$

$$(13)$$

7

where

$$\mathcal{L}_o = \frac{\partial^2}{\partial \xi^2} - \gamma^2 \tag{14}$$

$$\mathcal{L}_1 = \frac{\partial^2}{\partial \xi \partial \zeta'} - \gamma^2 \cos 2\beta \tag{15}$$

Enforcing the boundary condition that the tangential component of the total electric field vanish at the surface of the scatterer yields

$$-4\pi \epsilon_o \, s \, E_\xi^{inc}(\xi) = \int_0^L I_o(\xi') \mathcal{L}_o G_o(\xi, \xi') \, d\xi' + \int_0^L I_1(\zeta') \mathcal{L}_1 G_1(\xi, \zeta') \, d\zeta'$$

$$\tag{16}$$

Now the current at any point on the image, $I_1(\zeta')$, is equal in magnitude but opposite in sign to the current at that equivalent point on the scatterer itself. Hence, one may write $I_1(\zeta') \mathcal{L}_1 G_1(\xi, \zeta')$ in terms of the scatterer current and coordinates, and the integral equation becomes

$$-4\pi \epsilon_o \, s \, E_\xi^{inc}(\xi) = \int_0^L I_o(\xi') \left[\mathcal{L}_o G_o(\xi, \xi') + \overline{\mathcal{L}_1 G_1}(\xi, \xi') \right] d\xi' \tag{17}$$

where

$$\overline{\mathcal{L}_1} = \frac{\partial}{\partial \xi \partial \xi'} + \gamma^2 \cos 2\beta$$

and

$$\overline{G}_1(\xi, \xi') = \frac{e^{-\gamma \left[\left(\left| L-\xi-\xi' \right| \sin\beta - 2h \right)^2 + \left(\left| \xi-\xi' \right| \cos\beta \right)^2 \right]^{1/2}}}{\left[\left(\left| L-\xi-\xi' \right| \sin\beta - 2h \right)^2 + \left(\left| \xi-\xi' \right| \cos\beta \right)^2 \right]^{1/2}} \tag{19}$$

8

III. REDUCTION TO MATRIX EQUATION

Consider the wire element divided into subsections as shown in Figure 3. The unknown current is assumed to be-piecewise constant over each of these subsections, and according to the common thin-wire assumptions the current in the subsection at each end of the scatterer is assumed to vanish. A matrix equation of the form

$$\left[z_{mn} \right] \left[i_n \right] = \left[v_m \right] \tag{20}$$

may be obtained by substituting the piecewise constant current representation into equation (17) and forcing the resulting equation to be satisfied at a set of discrete match points defined as $\left| z_m \right|$ on Figure 3. As discussed by Harrington, the differential operators may be approximated by finite differences or the operations may be carried out analytically. In this particular approach, the $\mathcal{L}_o$ operator is replaced with finite difference operators, and the $\mathcal{L}_1$ operation is performed analytically. These operations yield the following definitions of the matrix elements in equation (20)

$$z_{mn} = \frac{1}{\Delta^2} \int_{\xi^n}^{\xi^{n+1}} \left[G_o \left(\xi_{m+1}, \xi' \right) - \left(\gamma^2 \Delta^2 + 2 \right) G_o \left(\xi_m, \xi' \right) + G_o \left(\xi_{m-1}, \xi' \right) \right.$$

$$\left. + \gamma^2 \Delta^2 \cos 2\beta \, G_1 \left(\xi_m, \xi' \right) + \Delta^2 \overline{G}_1{}''\left(\xi_m, \xi' \right) \right] d\xi', \quad \begin{array}{l} m=2, N-1 \\ n=2, N-1 \end{array}$$

$$\tag{21}$$

$i_n = \alpha_n$ (unknown coefficient of constant current
in the nth subsection), $\qquad$ n=z, N-1 $\quad$ (22)

$$v_m = - \frac{4\pi}{Z_o}\ \gamma E_o\ \sin \beta\ e^{-\gamma \xi_m \cos \theta}, \qquad m=2,\ N-1 \quad (23)$$

where

$$\Delta = \frac{L}{N-1} \text{ (N is the number of subsections} \qquad (24)$$
$$\text{on the scatterer)}$$

$$Z_o = \sqrt{\frac{\mu_o}{\epsilon_o}} \qquad (25)$$

and

$$\overline{G}''(\xi_m, \xi') = \overline{G}_1(\xi_m, \xi)\left[\left(\frac{\gamma}{R_1} + \frac{1}{R_1^2}\right)\cos 2\beta + \left(\frac{\gamma^2}{R_1^2} + \frac{3\gamma}{R_1^3} + \frac{3}{R_1^4}\right)\cdot\right.$$

$$\left.(L\sin^2\beta - 2h\sin\beta - \xi_m + \xi'\cos 2\beta)\cdot(L\sin^2\beta - 2h\sin\beta + \xi_m\cos 2\beta - \xi')\right]$$

$$(26)$$

$$R_1 = \left[\left(\left|L - \xi_m - \xi'\right|\sin\beta - 2h\right)^2 + \left(\left|\xi_m - \xi'\right|\cos\beta\right)^2\right]^{1/2} \quad (27)$$

IV. ALTERNATE FORMULATION USING EXACT EXPRESSIONS FOR THE ELECTRIC FIELD PRODUCED BY A CONSTANT CURRENT ELEMENT

The equation relating the tangential components of the incident and scattered field at the surface of the scatter is

$$-E_\xi^{inc}(\xi_m) = E_{o_\xi}^s(\xi_m) + E_{1_\xi}^s(\xi_m) \qquad (28)$$

10

where $E_{o_\xi}^s (\xi_m)$ and $E_{1_\xi}^s (\xi_m)$ are the components of the electric field produced at the surface of the scatterer by the wire current and charge and the image current and charge respectively. $E_{o_\xi}^s (\xi_m)$ may be determined from the vector and scalar potentials as outlined previously. However, it is convenient to determine $E_{1_\xi}^s (\xi_m)$ in a different manner. In the numerical solution presented in the previous section, the unknown current was represented as piecewise constant over a small subsection of the scatterer. The exact electric field produced by such a constant current element has been given by Harrington[9]. Using Harrington's expressions, one may determine $E_{1_\xi}^s (\xi_m)$ as

$$E_{1_\xi}^s (\xi_m) = \frac{Z_o \Delta}{2\pi} \sum_{n=2}^{N-1} \alpha_n e^{-\gamma r_{mn}} \left[\left(\frac{1}{r_{mn}^2} + \frac{1}{\gamma r_{mn}^3} \right) \cos \eta \cos \alpha \right.$$

$$\left. + \frac{1}{2} \left(\frac{\gamma}{r_{mn}} + \frac{1}{r_{mn}^2} + \frac{1}{\gamma r_{mn}^3} \right) \sin \eta \sin \alpha \right] \qquad (29)$$

where

$$r_{mn} = \left[\left(\left| L - \xi_m - \xi_n' \right| \sin \beta - 2h \right)^2 + \left(\left| \xi_m - \xi_n' \right| \cos \beta \right)^2 \right]^{1/2} \qquad (30)$$

$$\eta = \arctan \left[\frac{2h - (L - \xi_m - \xi_n') \sin \beta}{(\xi_m - \xi_n') \cos \beta} \right] - \beta, \quad m \neq n \qquad (31)$$

$$\eta = \frac{\pi}{2} - \beta, \quad m = n \qquad (32)$$

$$\alpha = \pi - \eta - 2\beta \qquad (33)$$

$$\xi_n' = (n-1) \Delta, \quad n = 2, N-1 \qquad (34)$$

11

The expression for $E^S_{o_\xi}(\xi_m)$ as determined in section III is

$$E^S_{o_\xi}(\xi_m) = \frac{Z_o}{4\pi\gamma\Delta^2} \alpha_n \sum_{n=2}^{N-1} \int_{\xi^n}^{\xi^{n+1}} \left[G_o(\xi_{m+1}, \xi') - (\gamma^2\Delta^2 + 2) G_o(\xi_m, \xi') + G_o(\xi_{m-1}, \xi') \right] d\xi'$$

Using these expressions for the scattered fields in equation (28), the matrix elements of equation (20) may be redefined as

$$z_{mn} = \frac{1}{\Delta^2} \int_{\xi^n}^{\xi^{n+1}} \left[G_o(\xi_{m+1}, \xi') - (\gamma^2\Delta^2 + 2) G_o(\xi_m, \xi') + G_o(\xi_{m-1}, \xi') \right] d\xi'$$

$$+ 2\Delta\gamma e^{-\gamma r_{mn}} \left[\left(\frac{1}{r_{mn}^2} + \frac{1}{\gamma r_{mn}^3} \right) \cos\eta \cos\alpha \right.$$

$$\left. + \frac{1}{2} \left(\frac{\gamma}{r_{mn}} + \frac{1}{r_{mn}^2} + \frac{1}{\gamma r_{mn}^3} \right) \sin\eta \sin\alpha \right] \tag{35}$$

$$i_n = \alpha_n \tag{36}$$

$$v_m = -\frac{4\pi}{Z_o} \gamma E_o \sin\beta \, e^{-\gamma \xi_m \cos\theta} \tag{37}$$

Note that the terms in equation (35) representing the contribution to the matrix element from the image are much simpler than the corresponding terms in equation (21). Both of these expressions for the elements of the coefficient matrix have been used in sample calculations, and good agreement between them is found. However, the time required to evaluate

12

equation (35) numerically was much less than the time required to evaluate equation (21). Hence all of the data presented here has been calculated using equation (35) as the definition of the elements of the coeffficient matrix.

V. SINGULARITY EXPANSION METHOD

Consider the matrix equation given by (20). This may be written in a slightly different form showing the dependence on the complex frequency, s, explicitly as

$$[Z(s)] \ [I(s)] \ = [V(s)] \tag{38}$$

where $[Z(s)]$ is an nxn matrix with the matrix elements defined by equation (35), $[I(s)]$ is an nx1 column matrix representing the unknown current coefficients, and $[V(s)]$ is an nx1 column matrix representing the excitation or source terms defined by equation (23).

Suppose one denotes the natural frequencies of the scattering system (scatterer with its image) as s_α. These natural frequencies are defined as those complex frequencies where the homogeneous matrix equation

$$[Z(s_\alpha)] \ [I(s_\alpha)] \ = [\, 0 \,] \tag{39}$$

has nontrivial solutions for $[I]$. This implies that the determinant of $[Z]$ must vanish at these natural frequencies. As pointed out by Tesche [5], several conclusions can be drawn about the nature of these singularities from a knowledge of response in the time domain. First, these natural resonances must occur in the left-half portion of the s-plane since currents which grow in time are not physically real. Second, the

13

singularities must occur in conjugate pairs since the current must be purely real in the time domain.

The solution to the original matrix equation (38) may be written symbolically as

$$[I(s)] = [Z(s)]^{-1}[V(s)], \qquad (40)$$

and the time domain solution as

$$[i(t)] = \frac{1}{2\pi j} \int_{\sigma_0 - j\infty}^{\sigma_0 + j\infty} [Z(s)]^{-1}[V(s)] \, e^{st} \, ds. \qquad (41)$$

Assume that the matrix $[Z(s)]$ can be represented by

$$[Z(s)]^{-1} = \sum_{\alpha} \frac{\left[R_\alpha\right]}{s - s_\alpha} \qquad (42)$$

where the sum is over all of the singularities in the s-plane. The matrix $[R_\alpha]$ is defined as the residue matrix at $s = s_\alpha$ and it calculated numerically in the same manner as in reference [5]. It has been shown that $[R_\alpha]$ may be represented as

$$[R_\alpha] = c_\alpha [M_\alpha]_0 [M_\alpha]_0^T \qquad (43)$$

where $[M_\alpha]_0$ is an nx1 column matrix defined as the natural mode vector (normalized in the same manner as defined by Tesche [5]) which solves the matrix equation

$$[Z(s_\alpha)] [M_\alpha]_0 = [0] \qquad (44)$$

and c_α, the normalization coefficient is defined as

$$c_\alpha = \frac{\left\{(r_\alpha)_{ij}\right\}}{\left\{(m_\alpha)_i\right\}_0 \left\{(m_\alpha)_j\right\}_0} \qquad (45)$$

where $\left\{(r_\alpha)_{ij}\right\}$, $\left\{(m_\alpha)_i\right\}$, and $\left\{(m_\alpha)_j\right\}_0$ are elements of the $[R_\alpha]$ and $[M_\alpha]_0$ matrices respectively.

14

With these definitions, the time response for the current on the scatterer may be determined according to the steps outlined in reference [5] . The final form is given by

$$[i(t)] = \sum_\alpha c_\alpha [M_\alpha]_o [M_\alpha]_o^T [U(t)] [V(s_\alpha)] e^{s_\alpha t} \qquad (46)$$

where [U(t)] is the Heaviside matrix discussed by Tesche [5] and defined here by

$$u_{kk}(t) = \begin{Bmatrix} 1 & , & t - \xi_k \cos \beta / c > 0 \\ 0 & , & t - \xi_k \cos \beta / c \leq 0 \end{Bmatrix} \qquad (47)$$

VI. NUMERICAL RESULTS

A computer code has been written to determine the natural resonances, mode vectors, and transient response for arbitrary orientations of the scatterer with respect to the ground plane. The techniques used in these calculations are the same as those discussed by Tesche [5]. The numerical data is essentially divided into two parts according to the geometry. The first group of curves is for the special case where the scatterer is parallel to the ground plane. The second group is for non-parallel orientation of the scatterer and the ground plane.

Before presenting data related to the ground plane problem, suppose we consider the scatterer in free space and look at the pattern of the singularities associated with its exterior natural resonances. These data have been presented in several of the references mentioned before, but they are repeated in Figure 4 for convenience.

15

The even and odd labeling of these singularities is determined by the spatial distribution of the mode function at the indicated complex frequency. Since the locations of these singularities are determined by a numerical search procedure, there is some question concerning whether all of the singular points in a given region have been located. An approach to answering this question is to consider the surface generated by some characteristic function having these same singular points. One such function for the problem at hand is defined by the magnitude of the determinant of the impedance matrix defined by an equation such as equation (35). Figure 5 is a plot of contour lines representing the relative magnitude of this characteristic function over some given region. The region considered in Figure 5 is the same region enclosed in dashed lines in Figure 4. The areas enclosed by tight circular contours vividly display the locations of the zeros of this characteristic function. This type of contour plot requires that the characteristic function be calculated at a set of points which adequately define the function in a given region. Although this information may be quite expensive in terms of computer time, one can locate all of the singularities in a given region at least within the accuracy of the grid size. The contours of Figure 5 were produced by a special contour plotting package, BRUT, furnished by Brown [10]. The characteristic function was calculated at 8100 points (a 90 x 90 matrix) to define the contours over the region shown.

Suppose we consider the case where the scatterer is parallel to the ground plane and fixed at a relative distance from the plane of $h/L = 0.5$. The location of the singularities (zeroes) of the characteristic function (defined as the magnitude of the determinant of the impedance matrix as given by equation (35)) are shown in Figure 6. These singularities form a distinct pattern in the sL/c

16

plane. The singularities lying in a nearly vertical layer near the imaginary axis represent natural resonances associated with the fundamental length of the scatterer itself. Some of the other singularities correspond to resonances associated with the two-body system formed by the scatterer and its image. Figure 7 shows the contours of the characteristic function for the region enclosed by dashes in Figure 6. Again the contour plot lends confidence that all of the singularities in the region have been located. The mode functions for each of the singularities of Figure 7 are given in Figure 8. For each of the singularities near either of the two axes, the imaginary part of the mode function is several orders of magnitude less than the real part, and hence the imaginary part is not shown at all.

With the scatterer fixed in this parallel orientation, it is interesting to observe the movements of the singularities as the relative separation between the scatterer and the ground plane is varied. Figures 9, 10, 11, 12, and 13 present the trajectories of the singularities associated with the natural resonances of the scatterer itself as a function of h/L. The behavior of these singularities is quite unusual. It might be expected that each of these trajectories would be a well-behaved spiral circling inward toward the free space location as h/L increased. However, as illustrated in the figures, this spiraling effect is rather quickly masked by the interaction of the spiraling singularity and other singularities which pass through the same region. Although other trajectories are not explicitly shown in Figures 10-13, additional calculations indicate that effects similar to those exhibited in Figure 9 are present in each of the regions considered by the other curves. The trajectories of some of the singularities associated with the resonances of the two-body system are presented in Figure 14. It appears that each of these singularities moves toward the origin as h/L increases. The

17

singularities which enter the region displayed by Figure 9 can easily be seen as they move into this same region set off by dashes on Figure 14.

Let us consider the region around the first resonant frequency of the scatterer (Figure 9) in more detail. As the parameter h/L becomes very small, the system formed by the scatterer and its image appear very much like an ideal two-wire transmission line where the frequency, $\omega L/c$ approaches π, and the radiation factor, $\sigma L/c$ approaches 0. As the parameter h/L increases, the singularity moves away from the imaginary axis and appears to be forming the inward spiral expected. However as h/L approaches two, this spiral deteriorates and the singularity swings out away from the imaginary axis and eventually turns downward and moves toward the origin. Simultaneously another singularity moves into the region of Figure 9 from above. A similar effect is seen as h/L approaches three. Additional calculations indicate that this interaction of the singularities occurs near all subsequent integer values of h/L. Another investigator, Wilton [11], has calculated the trajectories of the singularities which exist in this region for the thin-wire scatterer parallel to a ground plane. The results obtained independently by Wilton are shown in Figure 15. A comparison of the data given by Figures 9 and 15 indicates a small complex frequency shift in the trajectories but otherwise excellent agreement as to the general behavior of the singularities. These additional data by Wilton add credence to the presented results. As a further attempt to understand the behavior of the singularities in this region, a series of contour plots of the previously defined characteristic function for the region of Figure 9 is shown in Figure 16. Each of the figures is for a different value of h/L near 2.0. A similar set of contours is shown in Figure 17 for the same region but over a wider range of h/L. All of these contours

18

were produced in the same manner as previously discussed. The inter-actions of the singularities in this region are also dependent on the relative thickness of the scatterer. Figure 28 shows the trajectory of the singularity associated with the scatterer resonance as a function of h/L for four different shape parameters, $\Omega = 2 \ln(\ell/a)$. As the wire gets thinner, the trajectory of this singularity remains an inwardly con-verging spiral until larger values of h/L are reached. Another test was made in this same region of the sL/c plane to ascertain how the relative zone size in the moment solution affected the trajectories. Figure 19 illustrates the trajectory of the singularities for three different zone sizes. Due to the original assumption that the incident electric field is perpendicular to the ground plane, the scatterer cannot be excited in this parallel orientation, and, consequently, no time domain data has been calculated for this geometry.

Suppose we now consider cases where the scatterer is not parallel to the ground plane. In all of the data displaying natural frequencies and natural modes, the angle $\beta = \frac{\pi}{2} - \arccos (\sin \theta \cos \phi)$ is used to denote the angular orientation of the scatterer. Figure 20 shows the pole loca-tions for the case where h/L is fixed at 1.0 and the angle, β, varies from 0° (scatterer parallel to ground) to 90° (scatterer perpendicular to ground). Although all of the singularities which were found are plotted in Figure 20, other singularities may exist in the region which were not found. No attempt has been made to calculate contour information for the singulari-ties of the non-parallel orientations. The mode functions for each of these singularities are shown in Figure 21. As before, when the imaginary part is several orders of magnitude less than the real part, only the real part is given explicitly. The trajectories of the two singularities associated with the scatterer resonances nearest the origin are shown in Figures 22 and 23 as a function of β for several values of h/L.

The time history of the current induced on the scatterer for several typical geometries are illustrated in the next set of curves. In all of the cases to follow, the time histories are calculated using the contributions from the first five singularities associated with the scatterer resonances found nearest the origin. Figure 24 exhibits the time history of the current at three locations on the scatterer for $h/L = 0.75$ and $\beta = 30°$, $60°$, $90°$. A similar set of curves for $h/L = 1.0$ are given in Figure 25.

VII. COMPARISON WITH FOURIER INVERSION DATA

As mentioned in a previous section, the problem of scattering from a thin wire above a perfectly conducting ground plane has been solved by Tesche [8] using the method of moments to cast a Pocklington type integral equation into matrix form. The matrix equation was solved at a set of discrete frequencies, and this discrete frequency spectrum was transformed into the time domain by a numerical Fourier inversion scheme. In this section, data from that study is compared with data produced by the Singularity Expansion Method.

Figures 26 and 27 give plots of the time history of the current at two points on the scatterer for the case $h/L = 1.0$, $\phi = 0°$, $\theta = 90°$, $\Omega = 10.6$ $(L/a = 200)$. The solid curves are the results including the contributions from the first five cylinder resonances in the Singularity Expansion Method, and the dashed curves are those produced by Tesche [8] using time harmonic analysis with Fourier Inversion. Although the agreement between the curves is quite good, there appears to be a constant time shift between the two sets of data in Figures 26 and 27. A closer look at the two solution techniques does not indicate that any inherent time shift should be present. Consequently, the author has not identified the cause for this apparent shift.

Another interesting comparison can be made on the first resonant frequency and damping constant for the scatterer as a function of the

relative height and inclination of the wire with respect to the ground plane. Figure 28 is a plot of the percent change in the first resonant frequency relative to the free space resonant frequency as a function of h/L and β. The solid wave is reproduced from reference [8] and the discrete points designated with block symbols are Singularity Expansion data. Again the agreement is very good. The points produced by the Singularity Expansion Method basically represent a shift in the location of the first cylinder resonance relative to the location of the free space resonance. Hence, the data presented in Figure 28 is essentially taken from the information displayed in Figures 9 and 22. Figure 29 is a similar presentation of data for the damping constant of the first cylinder resonance. Figure 30 presents data for the damping constant of the first resonance as a function of β normalized by its value at $\beta = 90°$.

It might be pointed out that data such as displayed in Figures 28, 29, and 30 are produced quickly and directly using the Singularity Expansion Method; whereas, similar data resulting from a time-harmonic analysis must be obtained indirectly and often requires quite extensive calculations for obtaining good accuracy.

VIII. CONCLUSIONS

In carrying out the analysis presented here, several general observations have been made concerning the Singularity Expansion Method (SEM) as a solution technique for scattering problems. Most of these observations can be separated into two distinct classes: old questions answered by the SEM and new questions arising from the SEM. Other observations which might be categorized as comments or suggestions for future work are all lumped together in the final paragraph.

One interesting question about solution techniques in general is whether the solution technique being used is an efficient (both analytically and numerically) means for generating the specific data. Of course, the answer to this is directly dependent on the type of data required. Often in scattering problems, one is interested in the current and charge distributions induced on the scattering body as a function of both frequency and time. If this data is needed for only one particular set of parameters, then other techniques such as time harmonic analysis may be more attractive from an efficiency point of view. However, if data from several sets of parameters are required (such as a detailed parameter study), then the SEM is probably a much more efficient technique. This is particularly true if only the low frequency response or late time response is required since the SEM becomes more and more efficient as the number of singularities to be considered is reduced to a small number (3 or 4). Other types of data such as fundamental resonances and damping constants of a scattering system are often required. Although these may be obtained indirectly (and often inefficiently) by other solution techniques, they are basic necessities in the SEM and, consequently, are calculated directly (and often very efficiently). Such quantities of interest such as the shift in the fundamental resonance or damping constant as a function of one or more parameters are quite easy to calculate using the SEM. In contrast, if one is interested in the currents and charges at high frequencies and early times, the SEM becomes less and less attractive as the number of singularities to be considered gets large.

The data presented here indicates that the SEM can be used effectively to predict the response of two body scattering systems (or alternately one body over a ground plane) to incident electromagnetic radiation. In addition, the SEM allows one to separate the resonant frequencies and damping constants into those associated with the

22

fundamental dimensions of each of the two scattering bodies and those associated with the fundamental dimension between the two scattering bodies. These separate resonances and damping constants are invariably masked by techniques such as time harmonic analysis where the real frequency spectrum contains the desired information but does not yield specific numbers for these quantities without a great amount of work. The SEM also indicates that certain two-body scattering systems might be analyzed with a technique such as the perturbation method since the fundamental resonant frequencies (complex frequencies) and associated mode functions appear to be only slightly different from the same parameters of some known isolated scattering body. Another question answered in this analysis concerns the basic nature of the resonances of a two-body scattering system. Indeed it appears that the response of such systems can be characterized as a sum of simple damped sinusoids as has been predicted in previous investigations. No singularities of multiplicity greater than one were encountered nor were there any indications that contributions from branch cuts were required. For certain particular parameters, the singularities appeared to lie in distinct patterns which greatly facilitated the task of locating them precisely. Finally, as expected, contributions from only a few of the singularities were required to produce reasonably accurate (as compared with time-harmonic analysis) results for late times ($ct/L > 3$).

Several new questions were raised in applying the SEM to the analysis of the two-body scattering problem. A basic question arises concerning the location and identification of the resonances of scattering systems with complicated geometry. Although the system considered in this study does not qualify as complicated, many of the higher order resonances were most difficult to predict and locating them numerically was a tedious chore. If the determination of the fundamental resonances of scattering systems could be mathematically cast into a more

conventional problem such as eigen value determination or at least related in technique to problems of this type, then much of the guesswork of locating the singularities could be removed and the efficiency of the overall method could be greatly improved. The question of identifying each singularity with some basic physical interpretation of the scattering system under study is also raised. It is true that many of the resonances (complex) which lie near the $j\omega$-axis in the s-plane can be identified with exterior resonances of one or both of the scattering bodies, and in addition some of the resonances associated with the distance between the bodies may also be identified. However, in general, there seems to be no effective convention for labeling a given singularity to avoid the confusion of identity when that singularity moves into a region occupied by another singularity. If such a convention could be established which would allow the unique labeling of an arbitrary singularity, then much additional insight might be gained concerning the physical interpretation of the interactions between singularities. In addition to questions concerning the singularities themselves, the nature of the mode functions associated with each of the singularities is also puzzling. Although it seems quite apparent from their functional form that certain mode functions belong in the same general group, it is not so apparent as to what these groups mean in some physical sense. A systematic grouping of the mode functions into unique groups or classes could also lead to greater insight as to the actual physical processes taking place in the scattering system. Again it would seem that the categorization of the mode functions by a straightforward scheme would greatly simplify the problem of interpreting much of the data produced by the SEM.

Along with the subjects already mentioned, there are several other comments or suggestions concerning areas of interest for future work within the SEM. The following list of suggestions is by no

24

means complete, and many of the items are redundant from the previous paragraphs. However, they are repeated below for additional emphasis:

1) Extend the method to other geometries in order to gain additional insight into its applicability and its limitations,

2) Use the method in conjunction with some high-frequency technique such as the Geometrical Theory of Diffraction to develop a broad range of analysis,

3) Compare SEM results to results obtained from conventional techniques such as Perturbation Theory or Characteristic Mode Theory and explain how they are related,

4) Use the method to extract data such as natural resonances or time constants from experimental data or from theoretical data generated at some previous time,

5) Develop analytical and numerical techniques for relating the natural resonances to associated eigen values or at least to eigen value-type problems,

6) If possible, also relate the natural mode functions to corresponding eigen functions,

7) Establish a general convention for labeling the natural resonances and grouping the mode functions into unique classes,

8) Develop analytical or numerical techniques for determining which singularities should be included to achieve a desired accuracy or to extract some unique data such as contributions from secondary resonances or interaction resonances only,

9) Use the data produced by the SEM to synthesize the required response in some analytical or experimental system such as a loaded scatterer or radiator.

IX. REFERENCES

1.   Baum, C. E., "On The Singularity Expansion Method for the Solution of Electromagnetic Interaction Problems," EMP Interaction Note 88, December 1971.

2.   Marin, L. and Latham, R. W., "Analytical Properties of the Field Scattered by a Perfectly Conducting, Finite Body," EMP Interaction Note 92, January 1972.

3.   Lee, S. W. and Leung, B., "The Natural Resonance Frequency of a Thin Cylinder and Its Application to EMP Studies," EMP Interaction Note 96, February 1972.

4.   Marin, L., "Application of the Singularity Expansion Method to Scattering from Imperfectly Conducting Bodies and Perfectly Conducting Bodies Within a Parallel Plate Region," EMP Interaction Note 116, June 1972.

5.   Tesche, F. M., "On the Singularity Expansion Method as Applied to Electromagnetic Scattering From Thin-Wires," EMP Interaction Note 102, April 1972.

6.   Martinez, J. P., Pine, Z. L., and Tesche, F. M., "Numerical Results of the Singularity Expansion Method as Applied to a Plane Wave Incident on a Perfectly Conducting Sphere, EMP Interaction Note 112, May 1972.

7.   Marin, L., "Natural-Mode Representation of Transient Scattering From Rotationally Symmetric Perfectly Conducting Bodies and Numerical Results for a Prolate Spheroid," EMP Interaction Note 119, August 1972.

8.   Tesche, F. M., "Numerical Determination of the Step Wave Response of a Thin-Wire Scattering Element Arbitrarily Located Above a Perfectly Conducting Ground Plane," EMP Sensor & Simulation Note 141, Feb. 1972.

9.   Harrington, R. F., Time-Harmonic Electromagnetic Fields, Ch. 2, McGraw-Hill, Inc., 1961.

10.   Brown, T. L., "BRUT-A System of Subroutines for the Generation of Contours," Mathematics Note 26.

11.   Wilton, D. R., private communication.
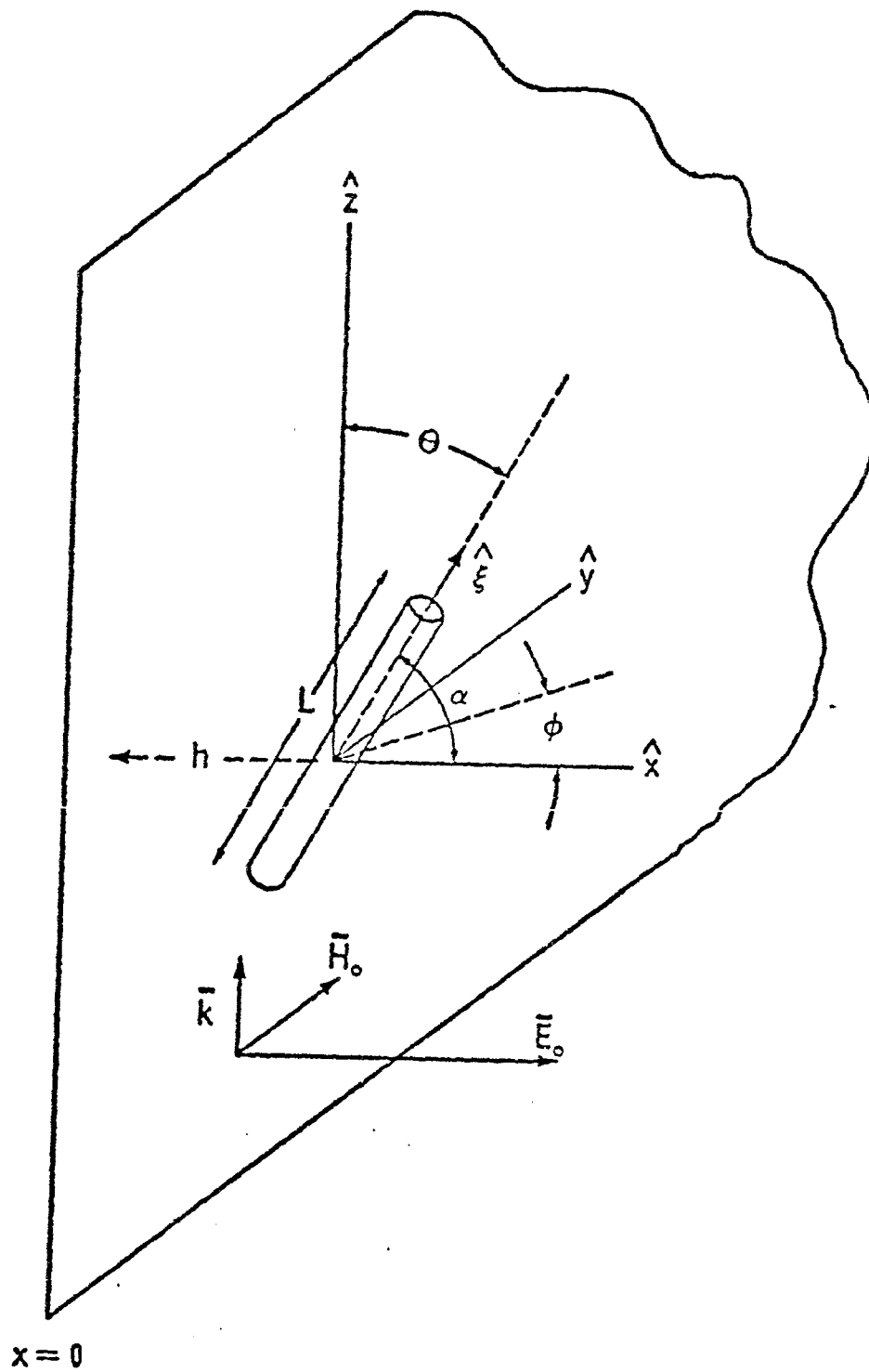
Figure 1. Thin-wire scatterer arbitrarily oriented above
a perfectly conducting ground plane.

27
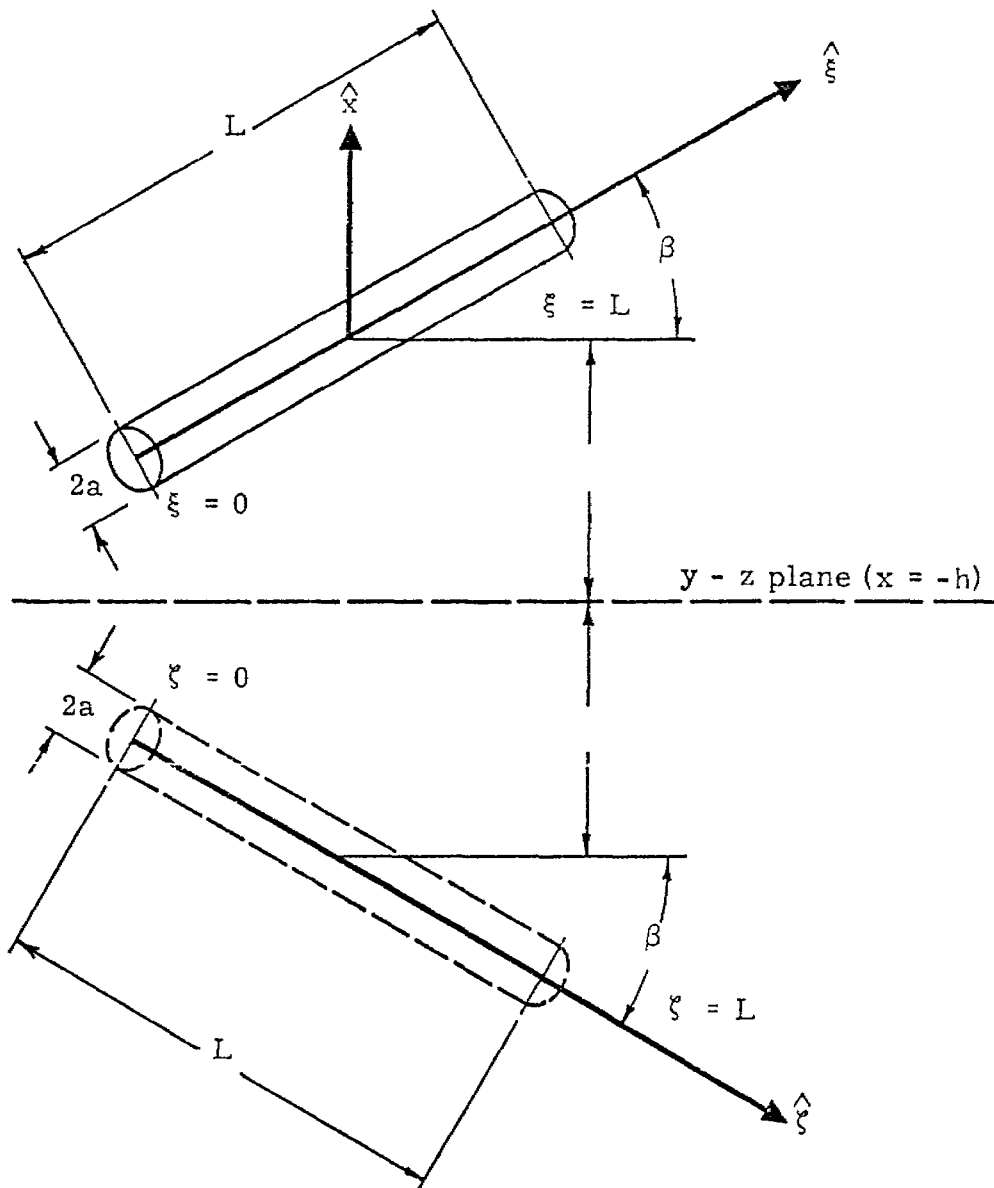
Figure 2. Orientation of the scatterer and its image
in terms of the angle β.

28

ξ^{N+1}

ξ^N

$\xi_N = L$

ξ^{n+1}

ξ^n ξ^m

$\xi_m = (m-1)\,\Delta, \ m = 1, N$

$\xi^n = (n - \frac{3}{2})\,\Delta, \ n = 1, N+1$

$\Delta = \dfrac{L}{N-1}$

ξ^3

ξ^2 ξ_2

ξ^1 $\xi_1 = 0$

β
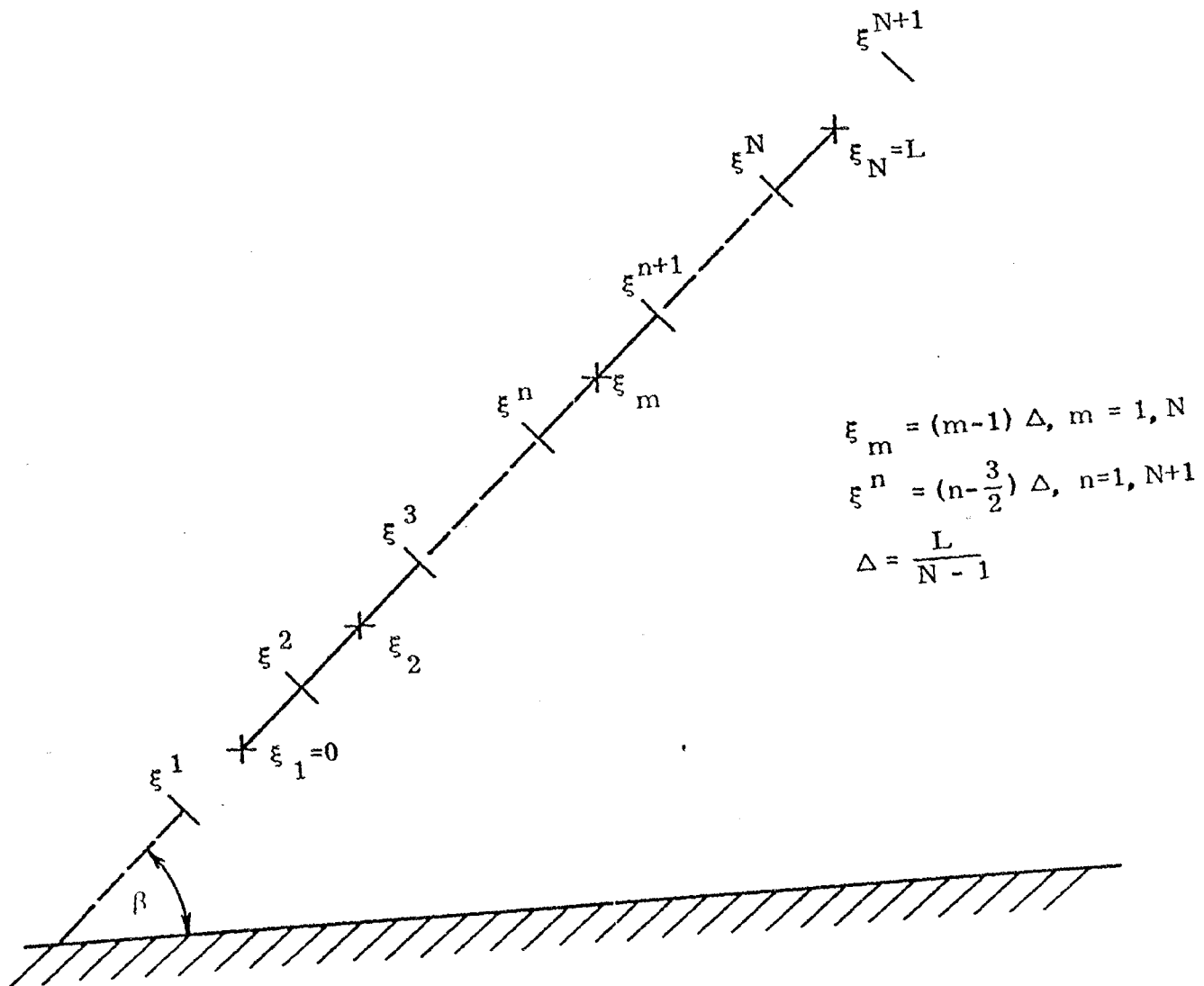
Figure 3. Scatterer divided into N zones with a match point centered in each zone.
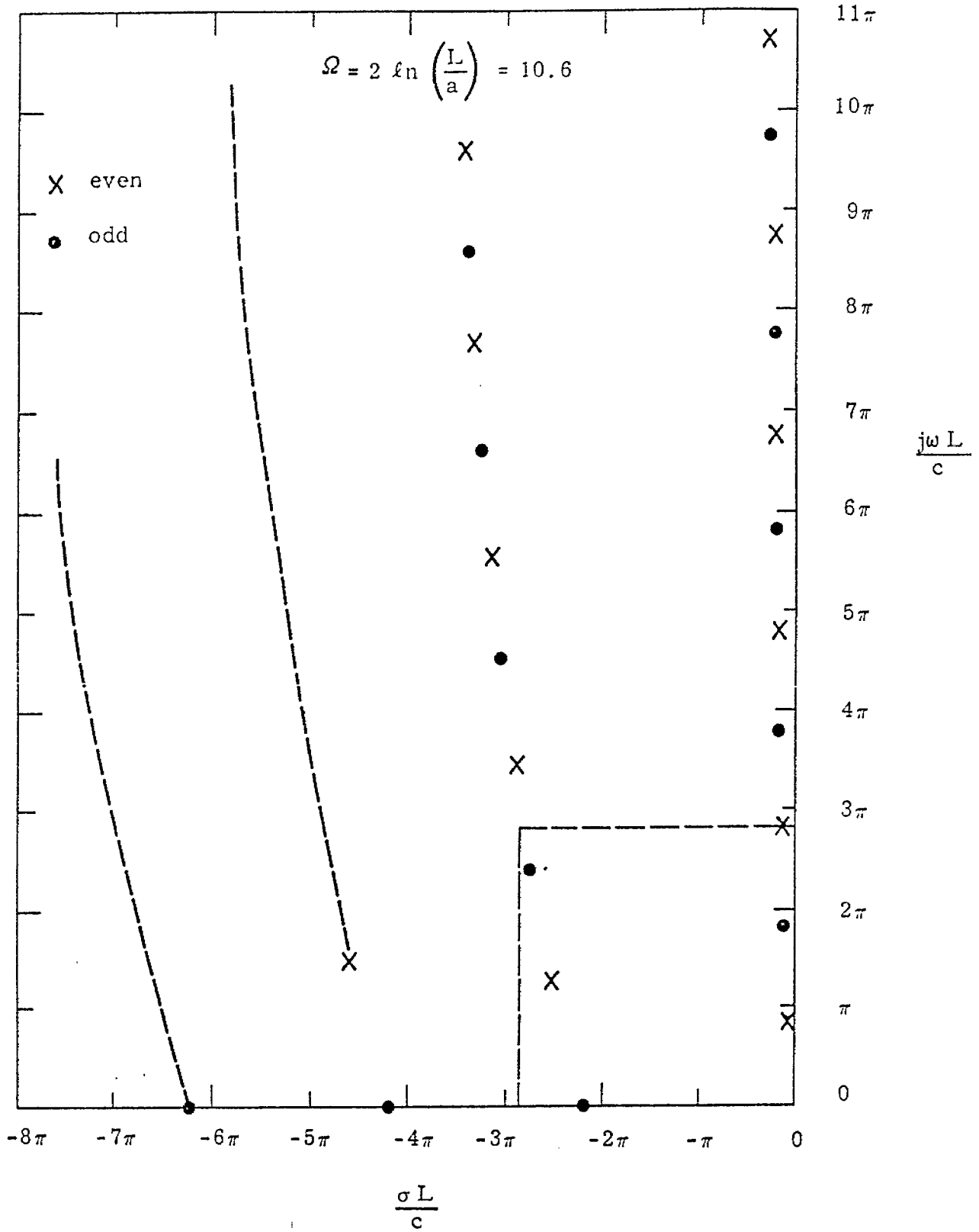
Figure 4. Location of the singularities of a thin-wire
scatterer in free space.
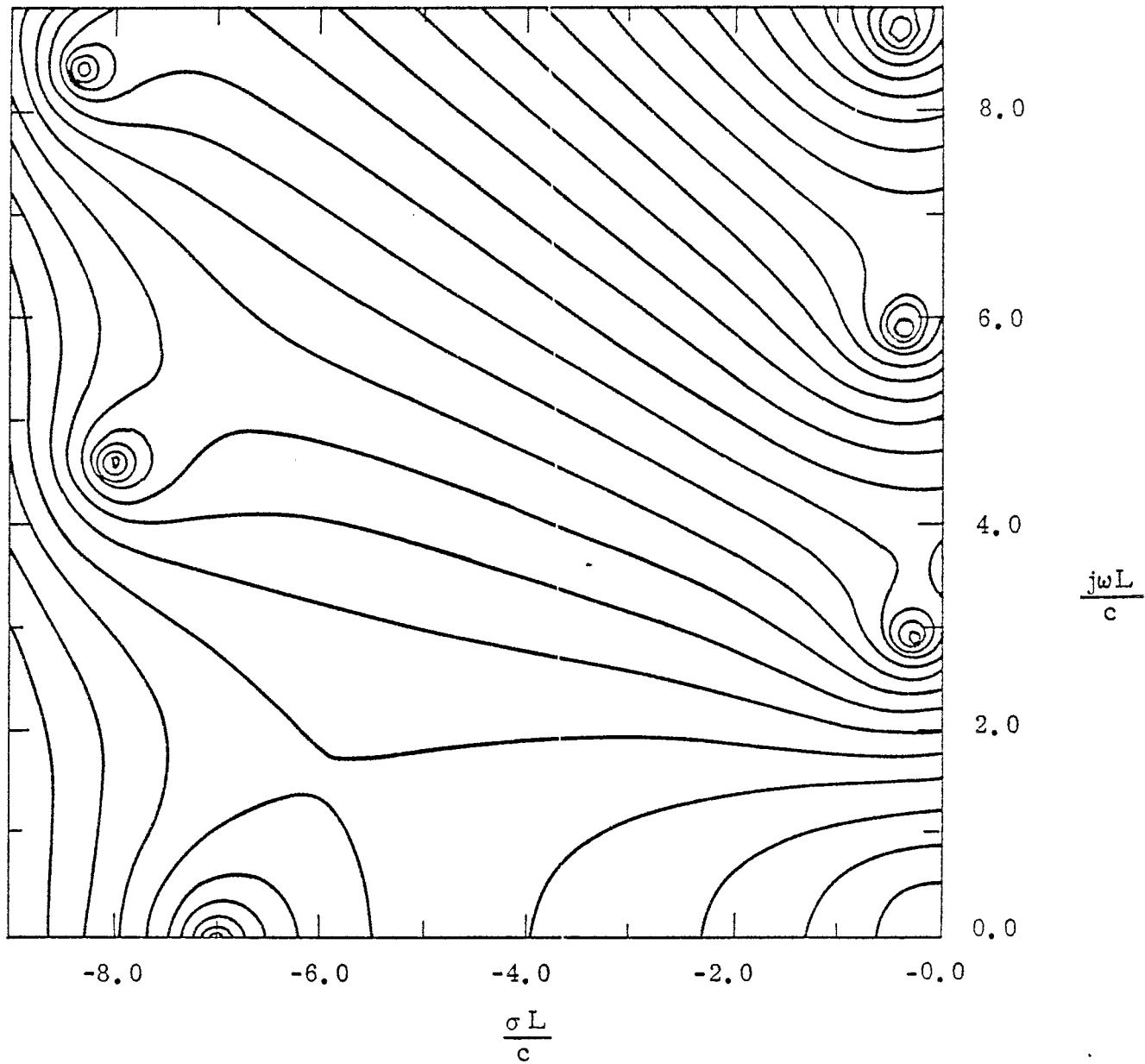
Figure 5. Contours of the characteristic function for a thin-wire in free space (Ω = 10.6, L/a=200).
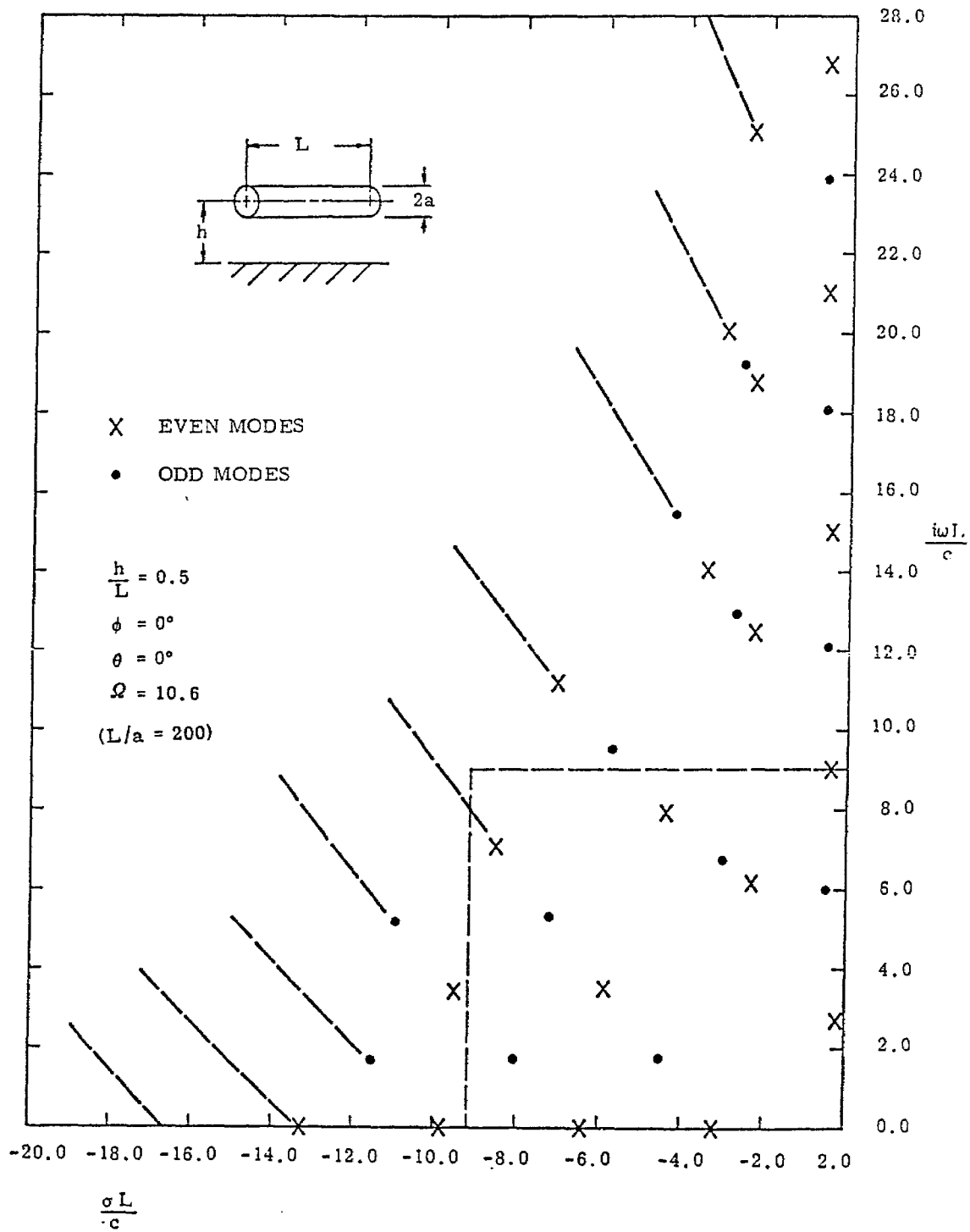
Figure 6. Location of the singularities of the thin-wire scatterer above a ground plane.
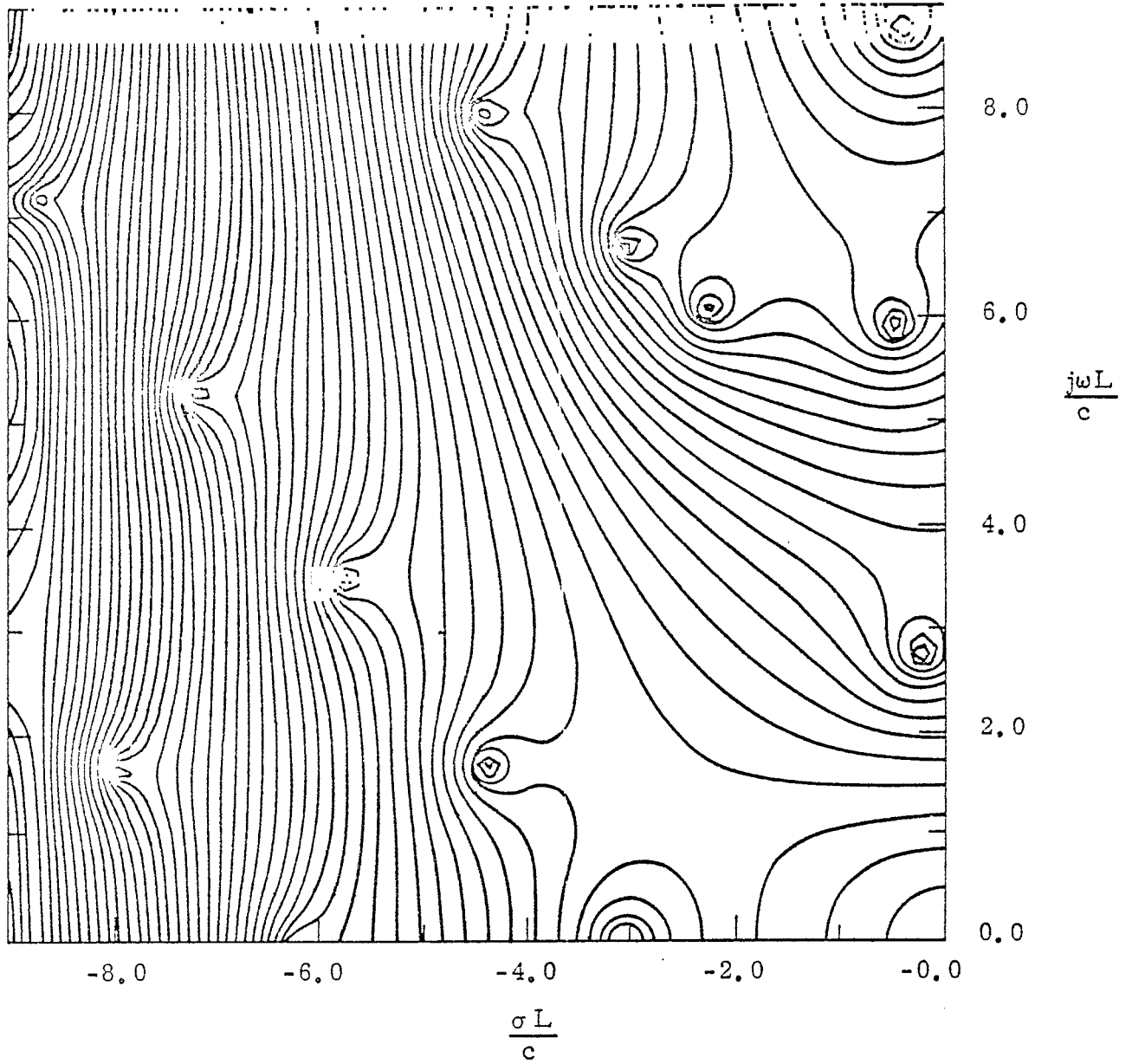
Figure 7. Contours of the characteristic function for a thin-wire
scatterer above a ground plane (h/L = 0.5, θ = 0°,
ϕ = 0°, Ω = 10.6, L/a = 200).

33
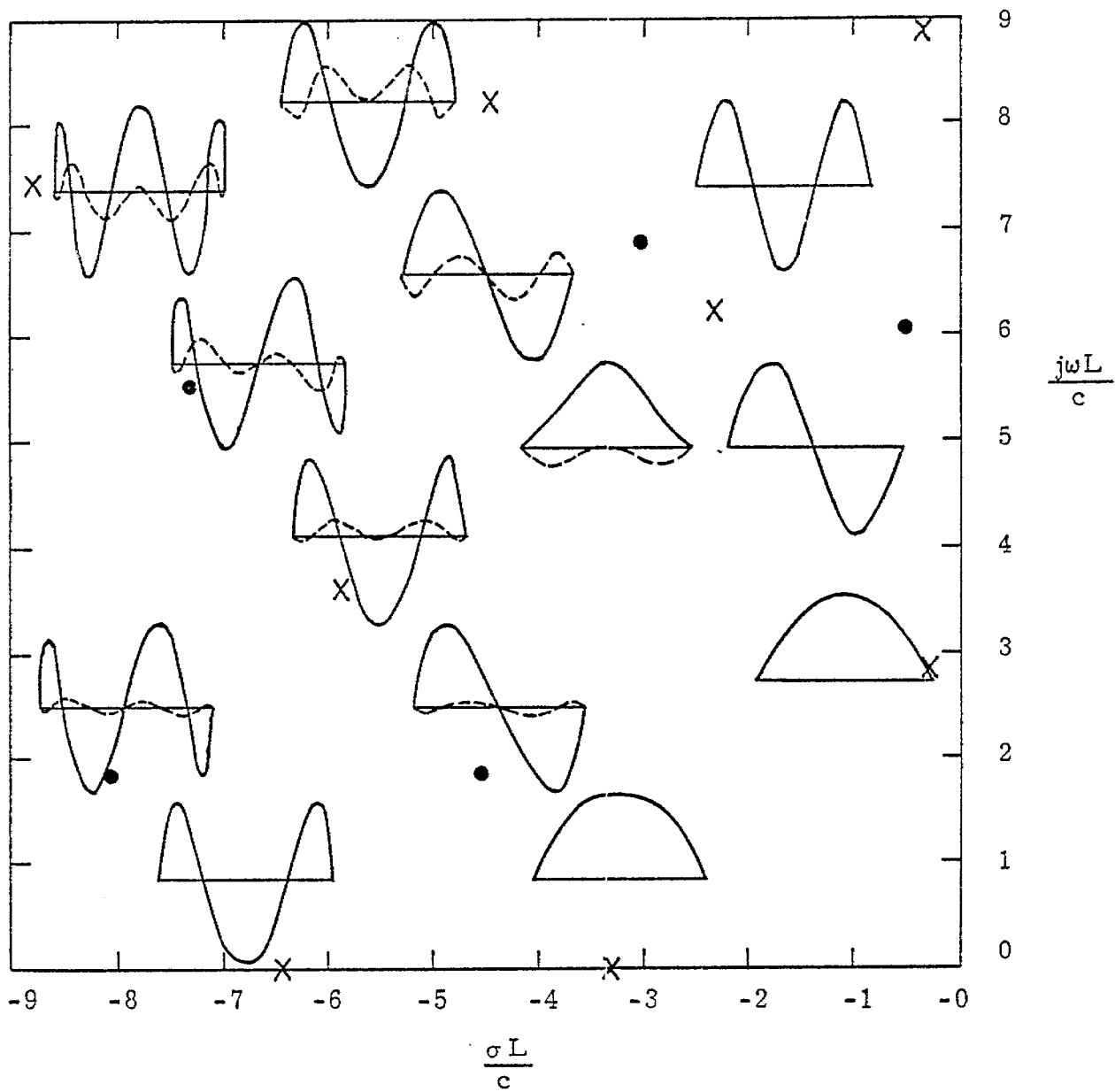
Figure 8. Mode functions for the singularities in the region
shown in Figure 7 (h/L = 0.5, ϕ = 0°, Ω = 10.6,
L/a = 200).

34
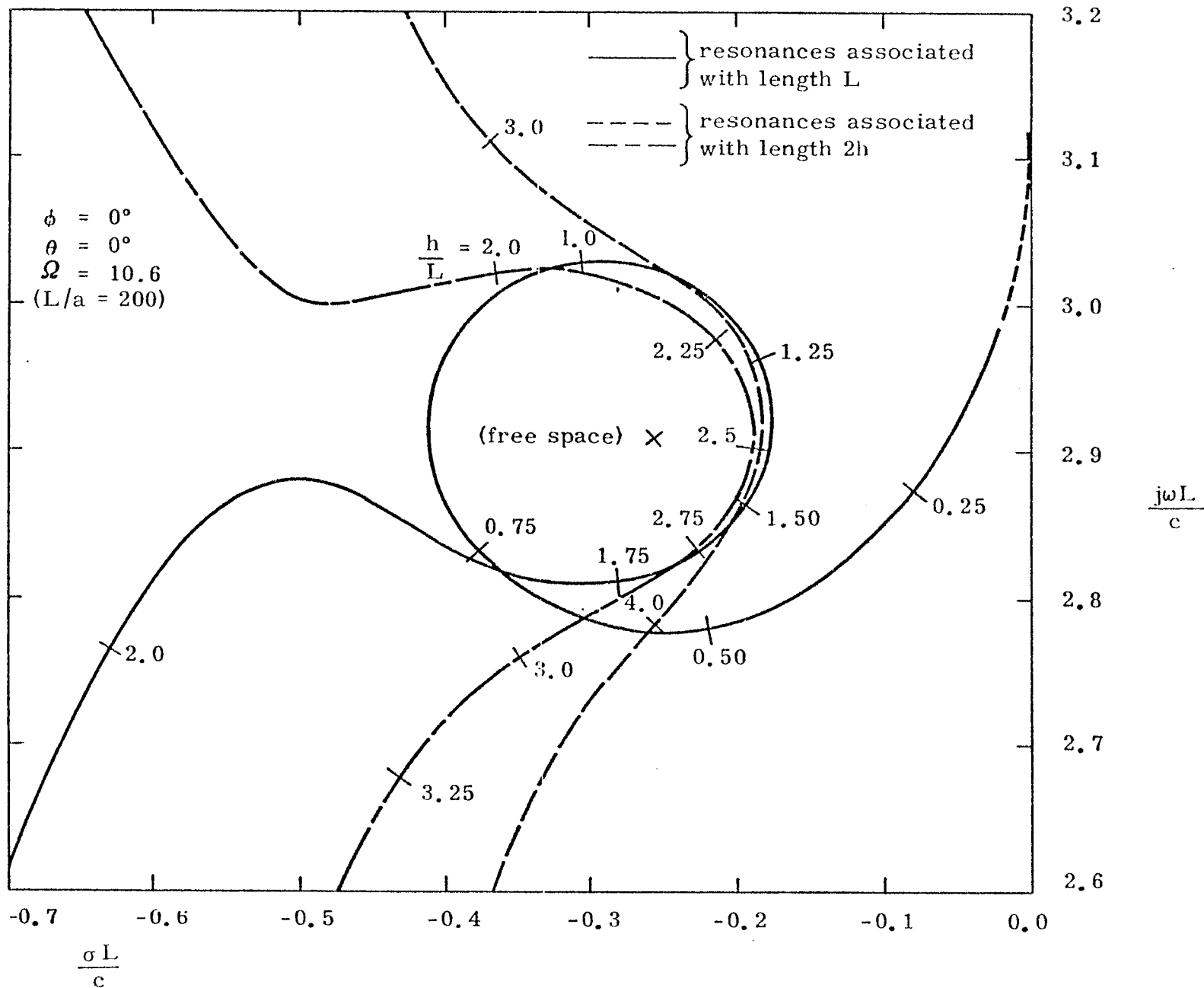
Figure 9. Trajectory of the singularity associated with the
first resonance of the scatterer itself.
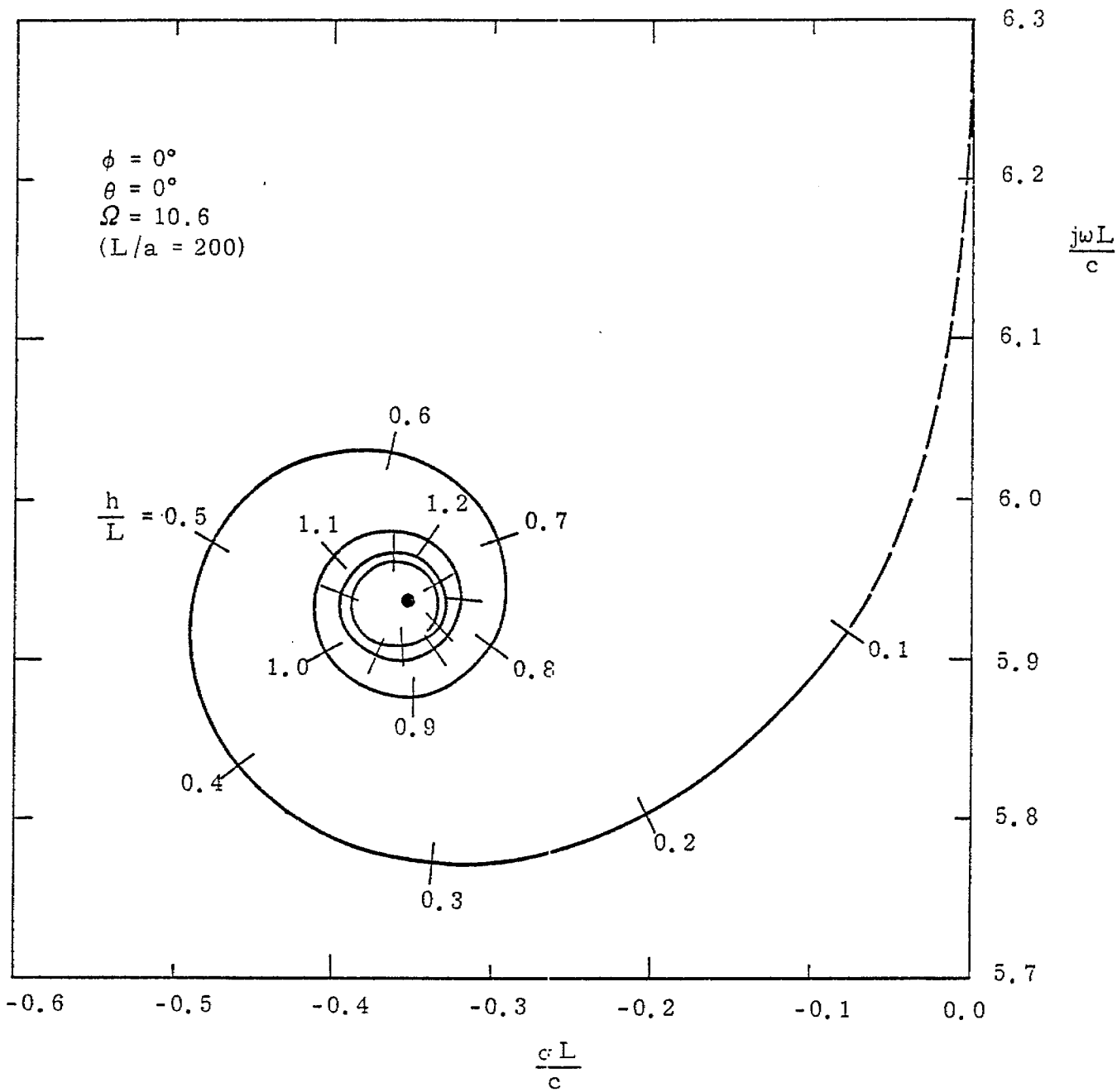
Figure 10. Trajectory of the singularity associated with the
second resonance of the scatterer itself.
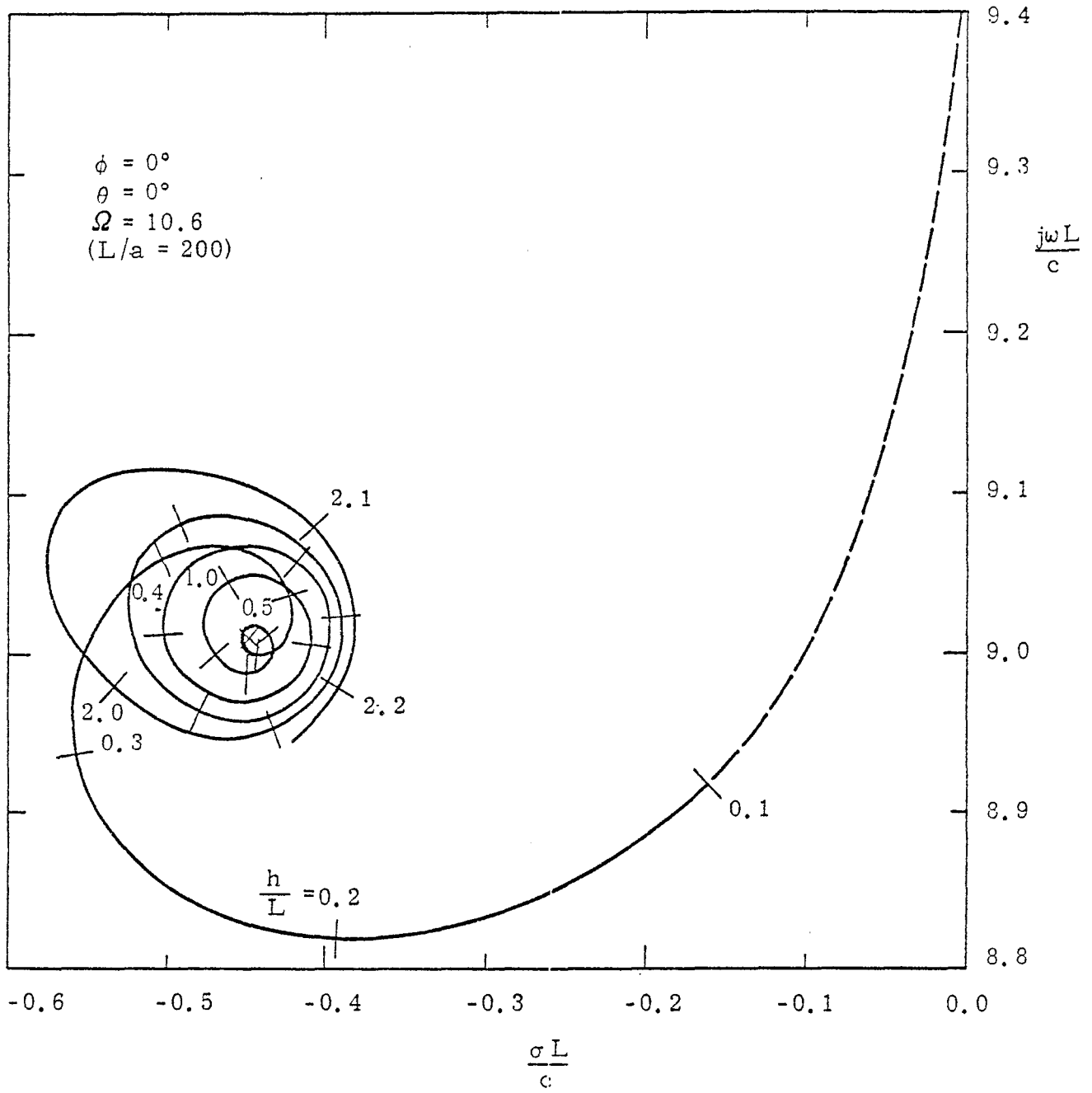
Figure 11. Trajectory of the singularity associated with the third resonance of the scatterer itself.
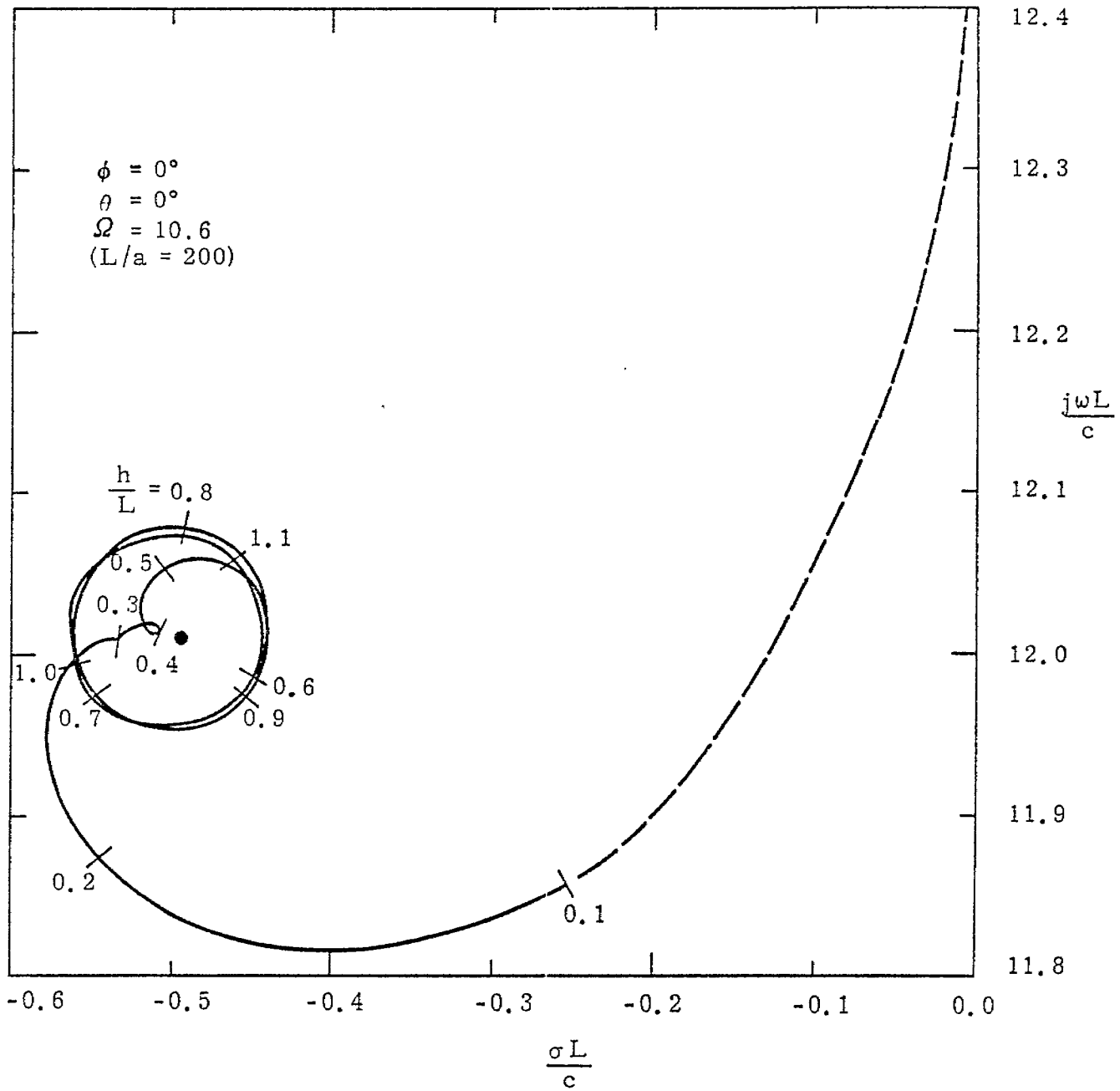
Figure 12. Trajectory of the singularity associated with the
fourth resonance of the scatterer itself.

$\phi = 0°$
$\theta = 0°$
$\Omega = 10.6$
$(L/a = 200)$

$\dfrac{h}{L} = 0.4$
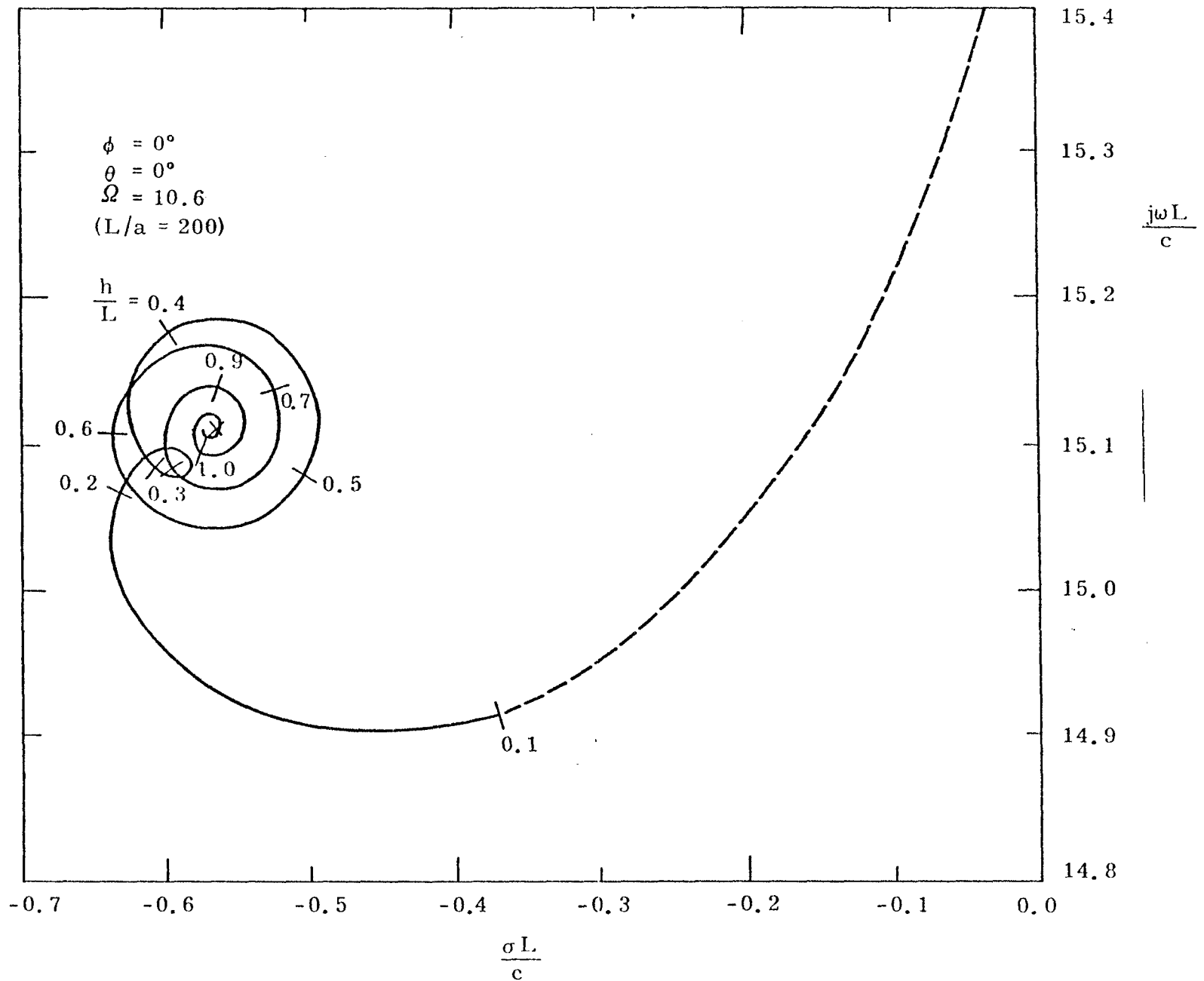
Figure 13. Trajectory of the singularity associated with the fifth resonance of the scatterer itself.

39
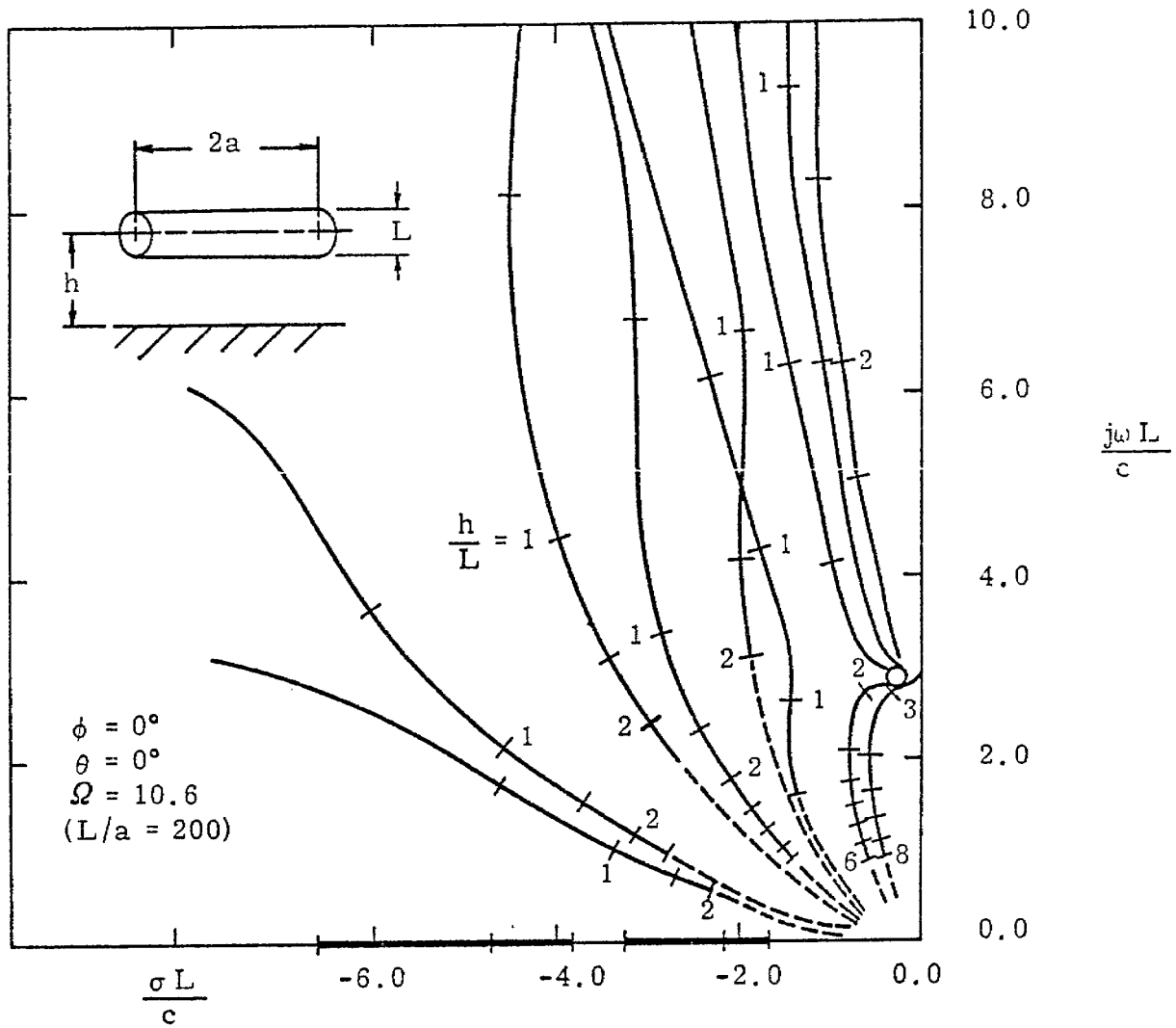
Figure 14. Trajectories of some of the singularities associated with the resonance of the two-body system.
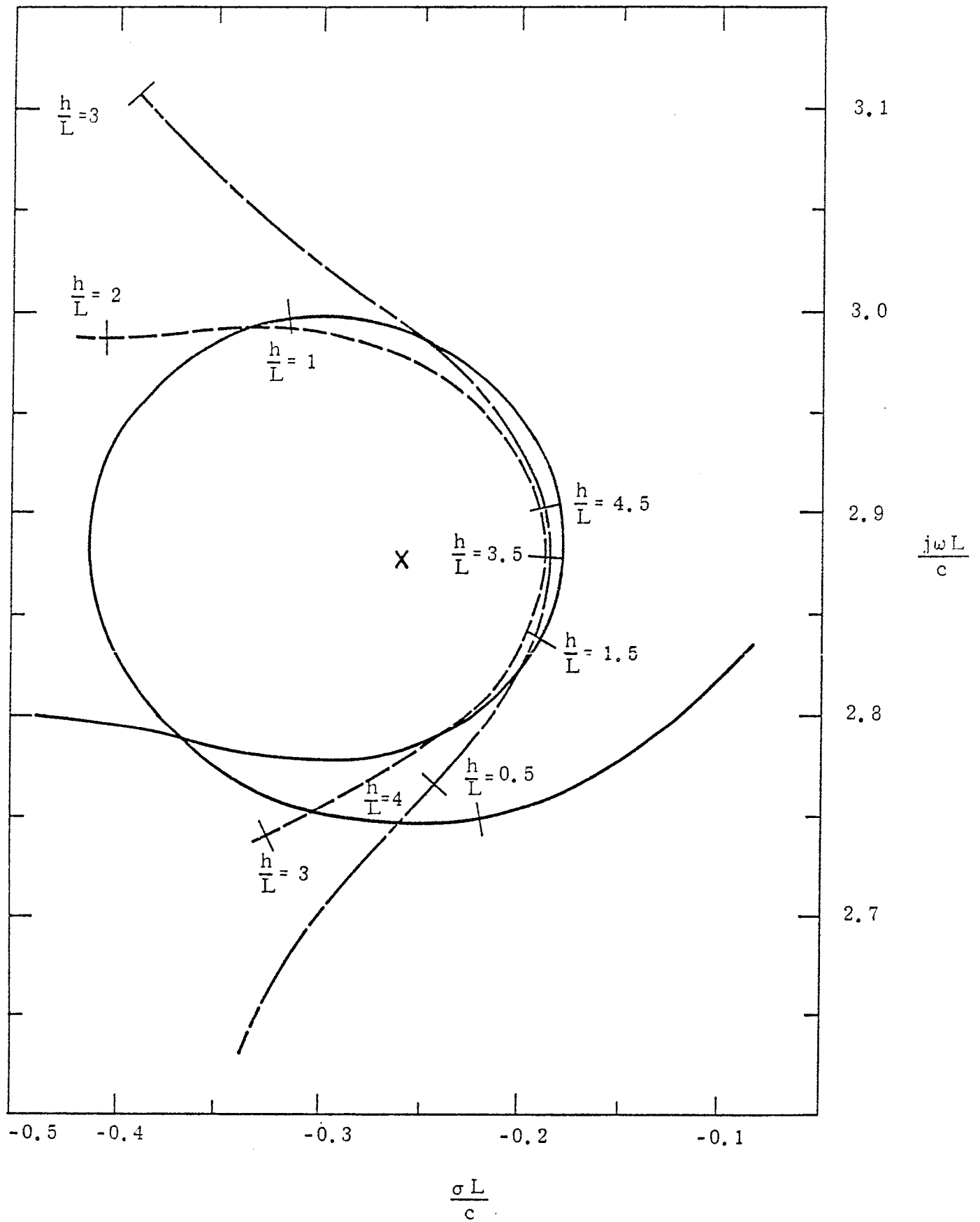
Figure 15. Trajectories of the singularities shown in Figure 9
as determined by Wilton [11] .
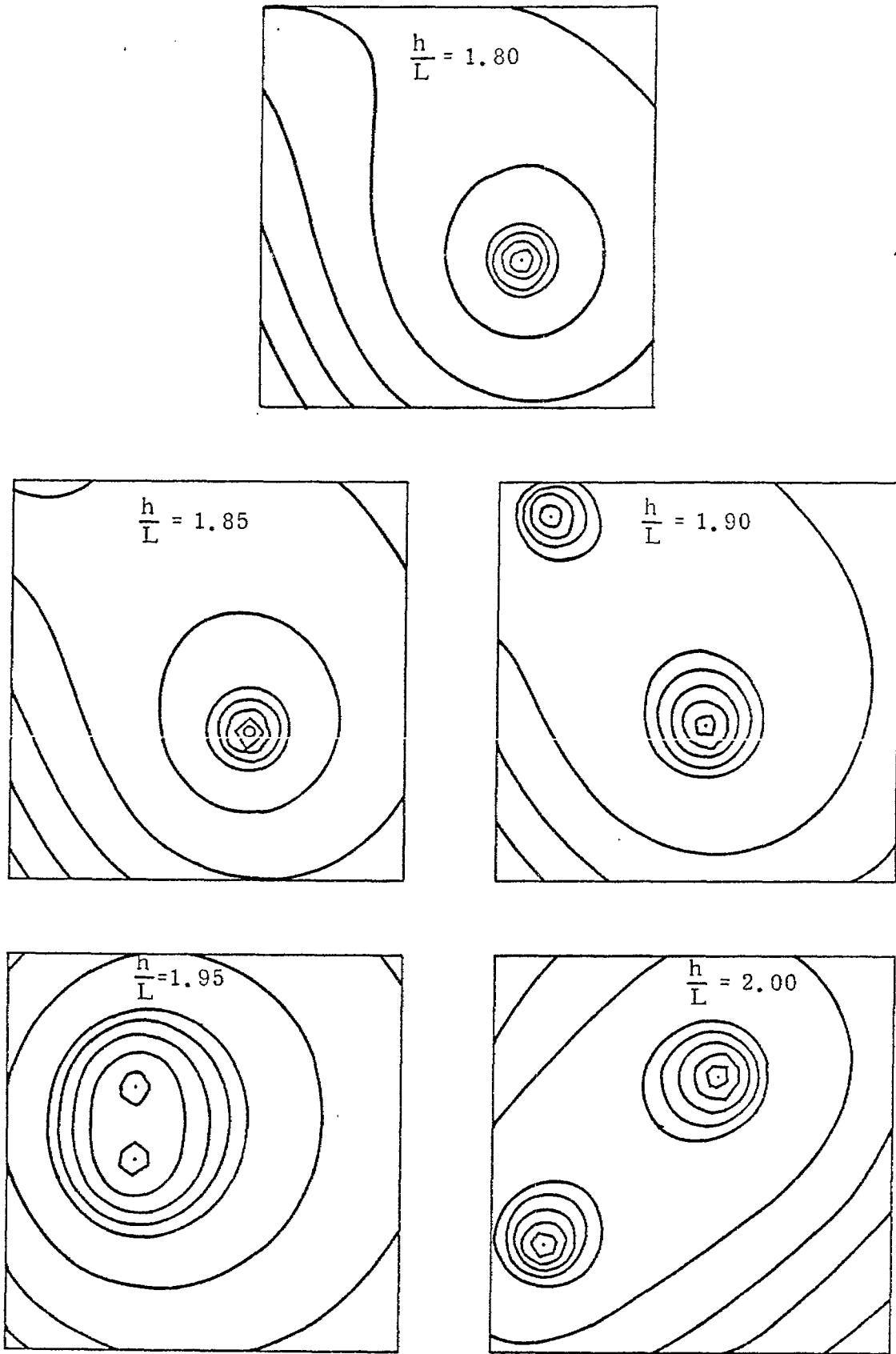
Figure 16. Contours of the region near the first scatterer singularity for values of h/L from $1.80 \xrightarrow{(0.05)} 2.00$.
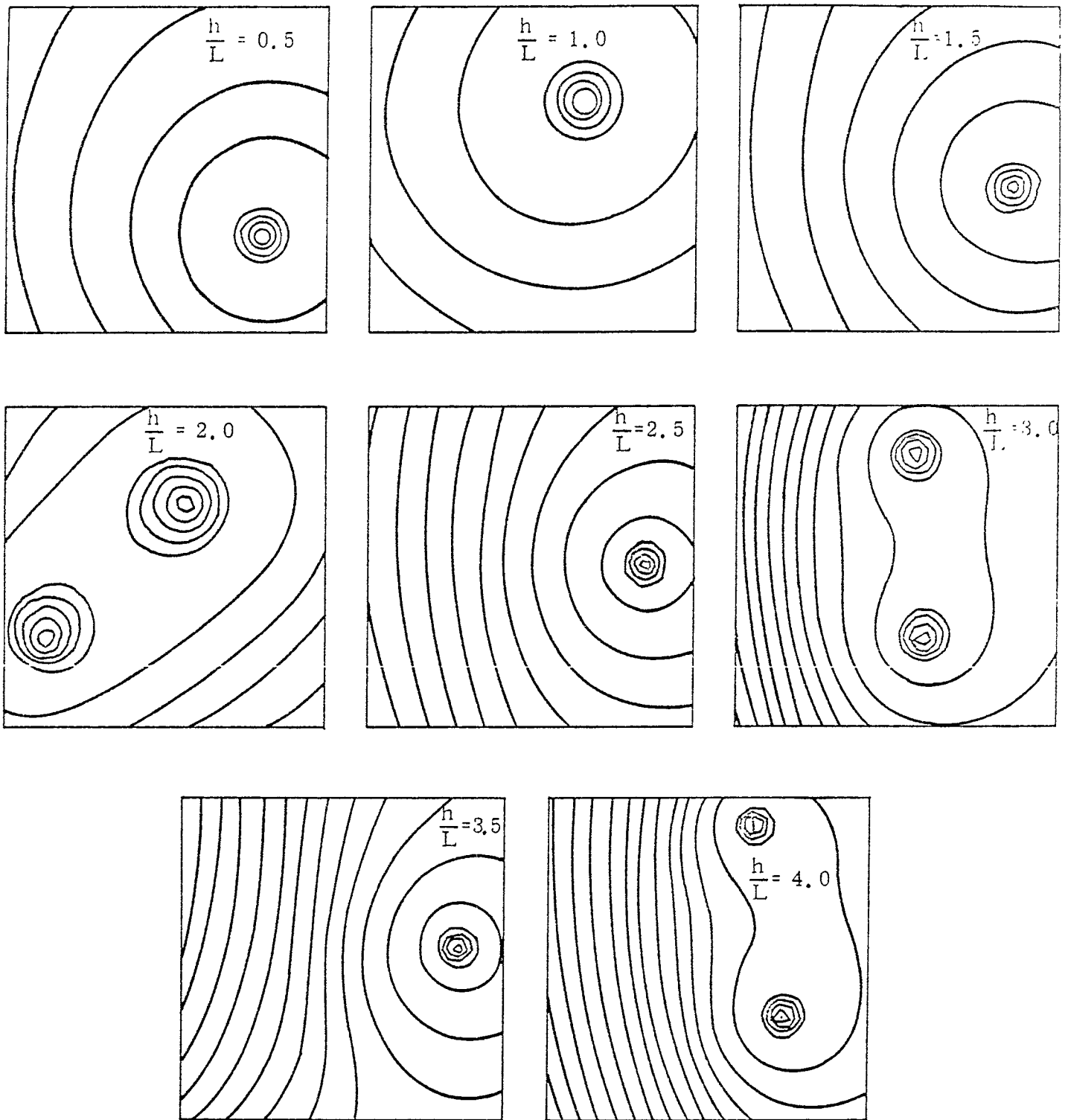
Figure 17. Contours of the region near the first scatterer singularity
for value of h/L from $0.5 \xrightarrow{(0.5)} 4.0$.
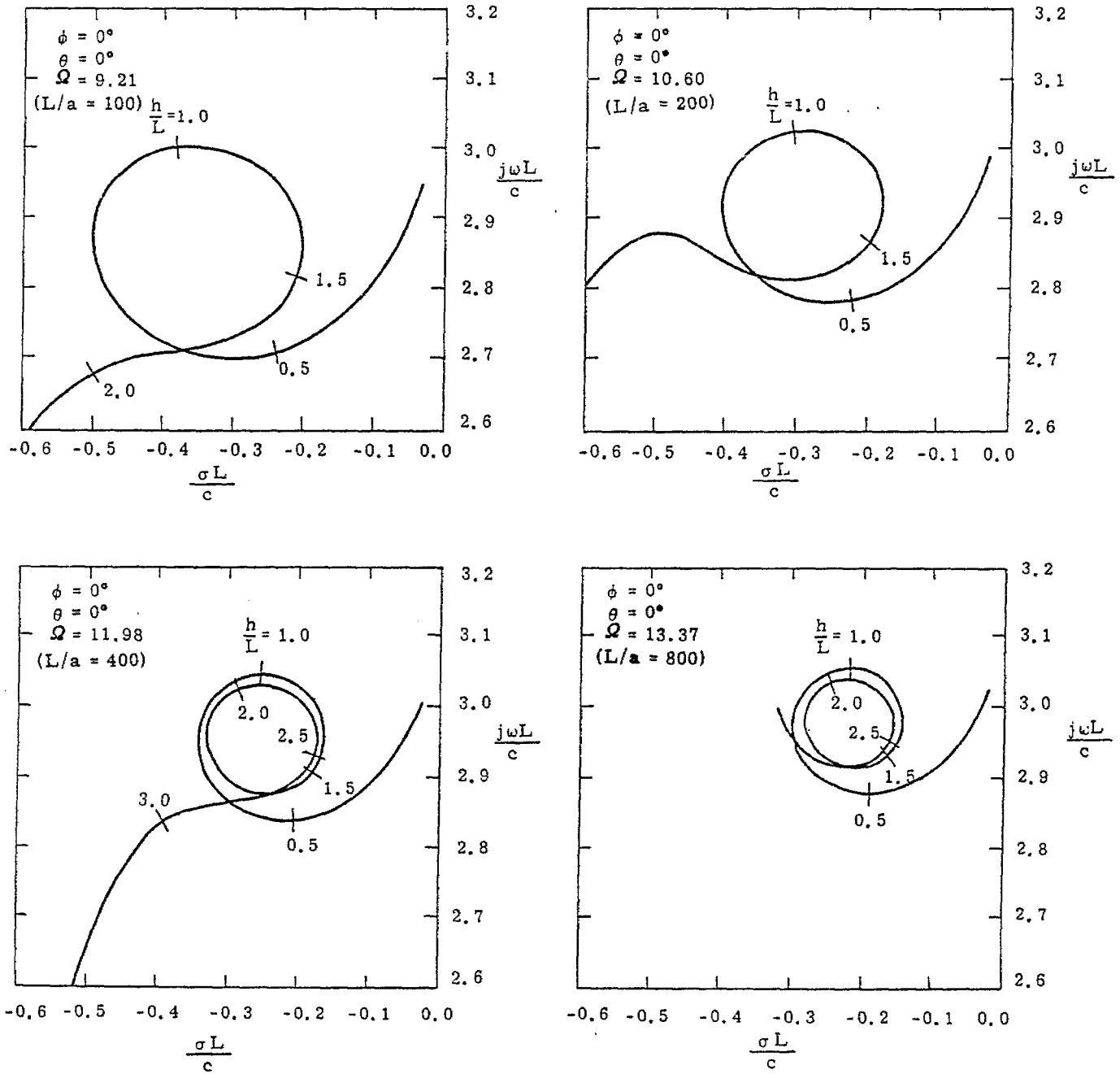
Figure 18. Trajectories of the first scatterer singularity for several values of the shape parameter, $\Omega = 2 \ln (L/a)$.

44
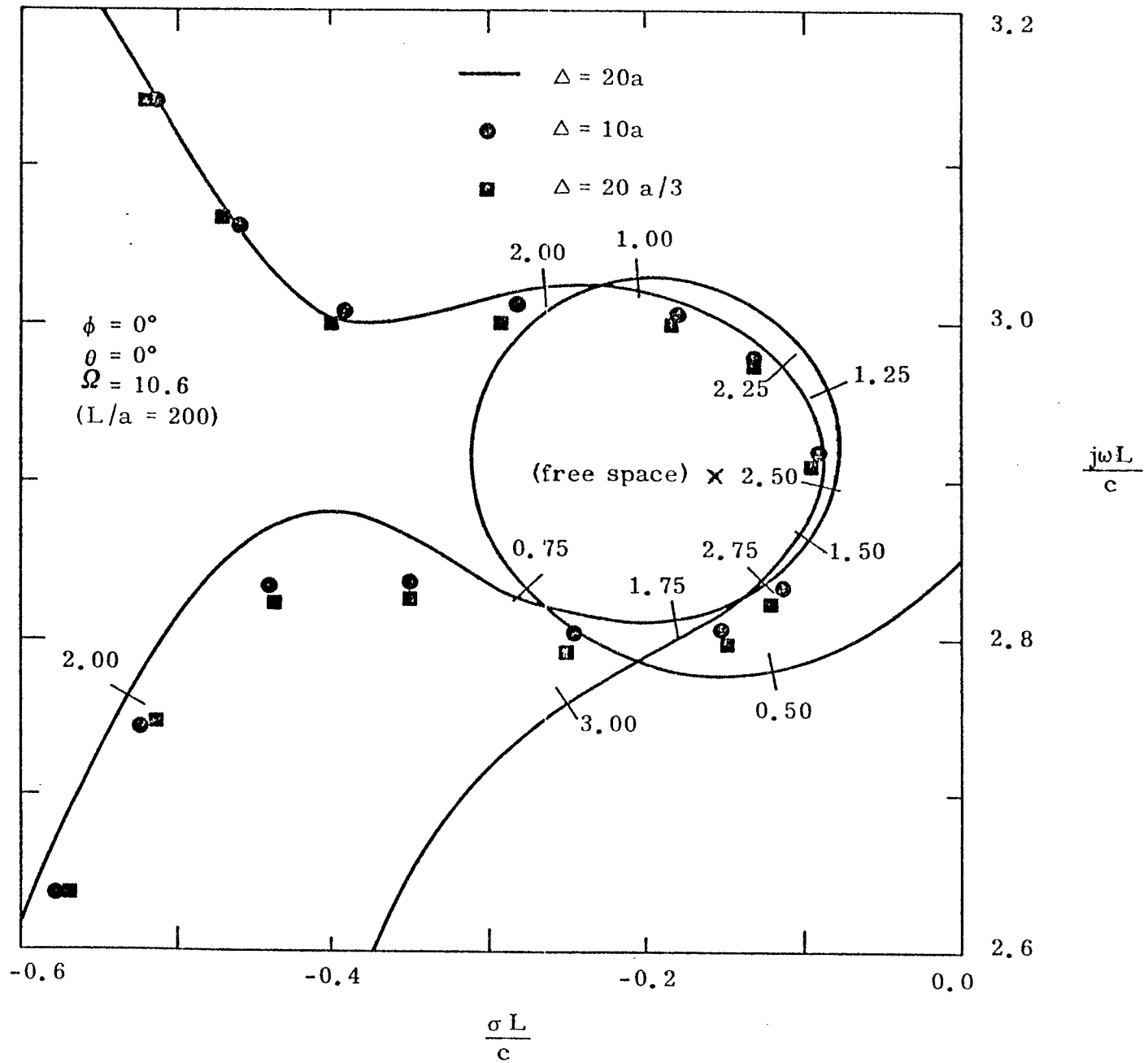
Figure 19. Trajectory of the first scatterer singularity
as a function of h/L and Δ .
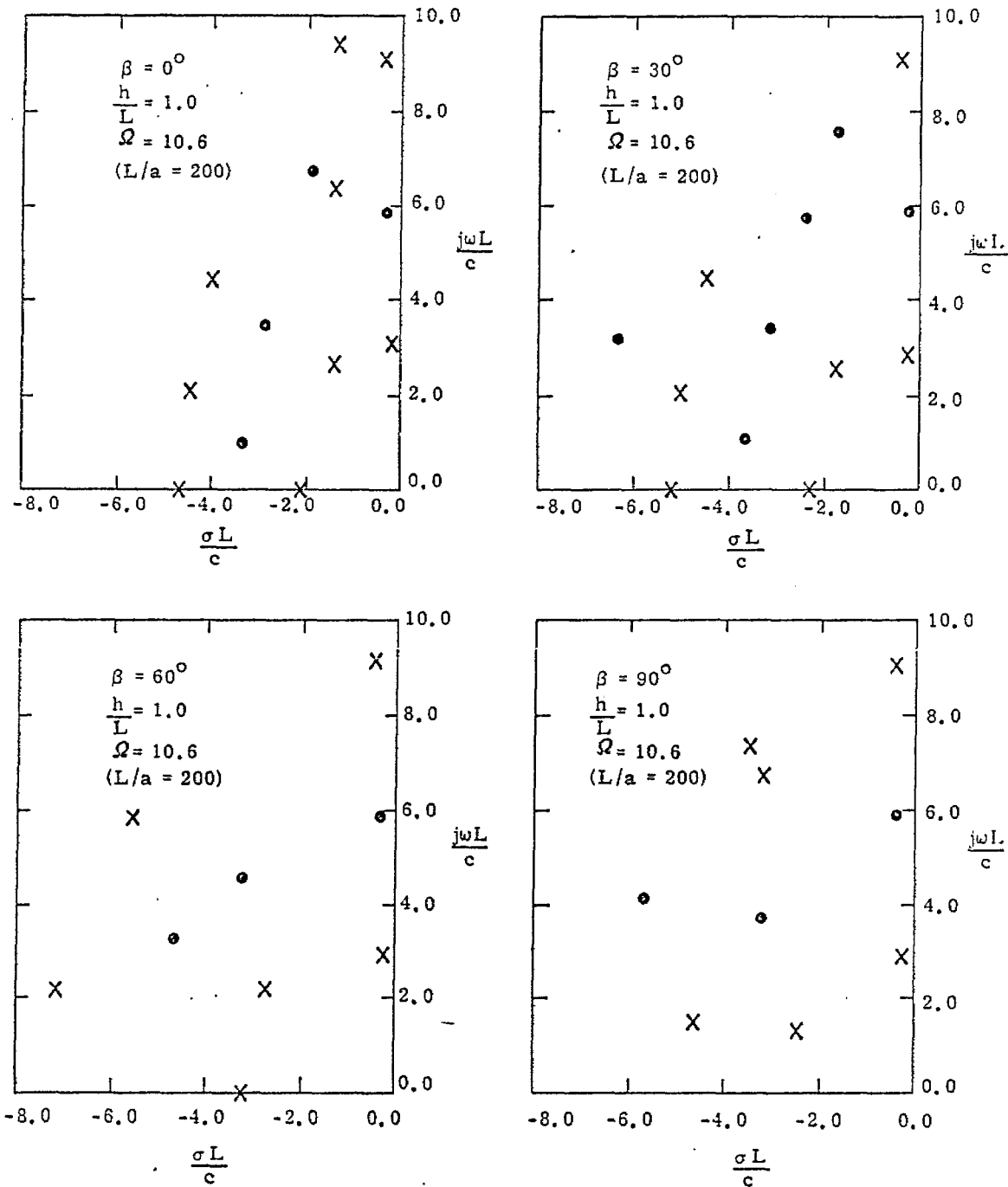
Figure 20. Locations of the singularities of the scatterer above the ground as a function of β.

46
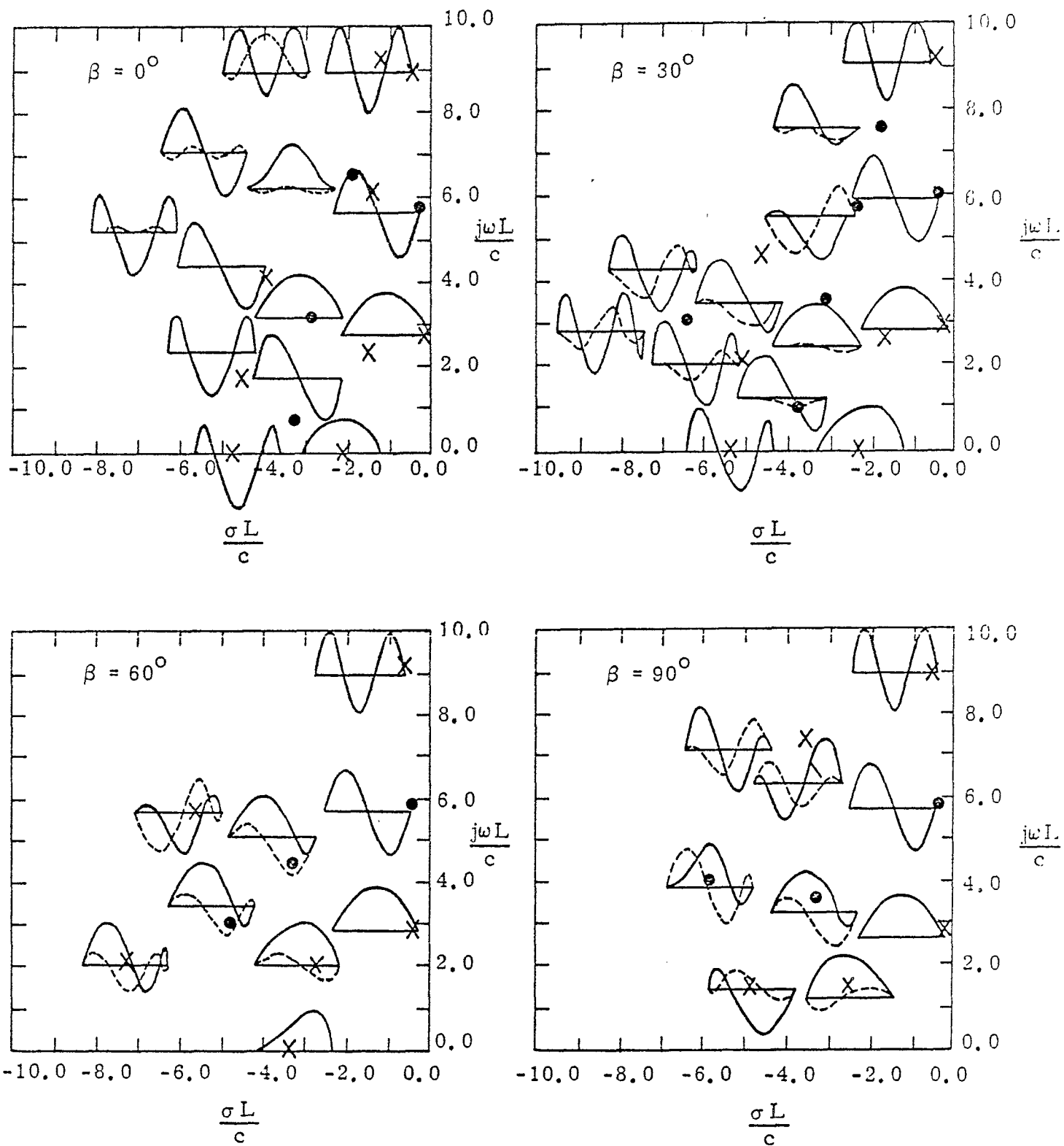
Figure 21.   Mode functions for the singularities shown in
Figure 20.

47
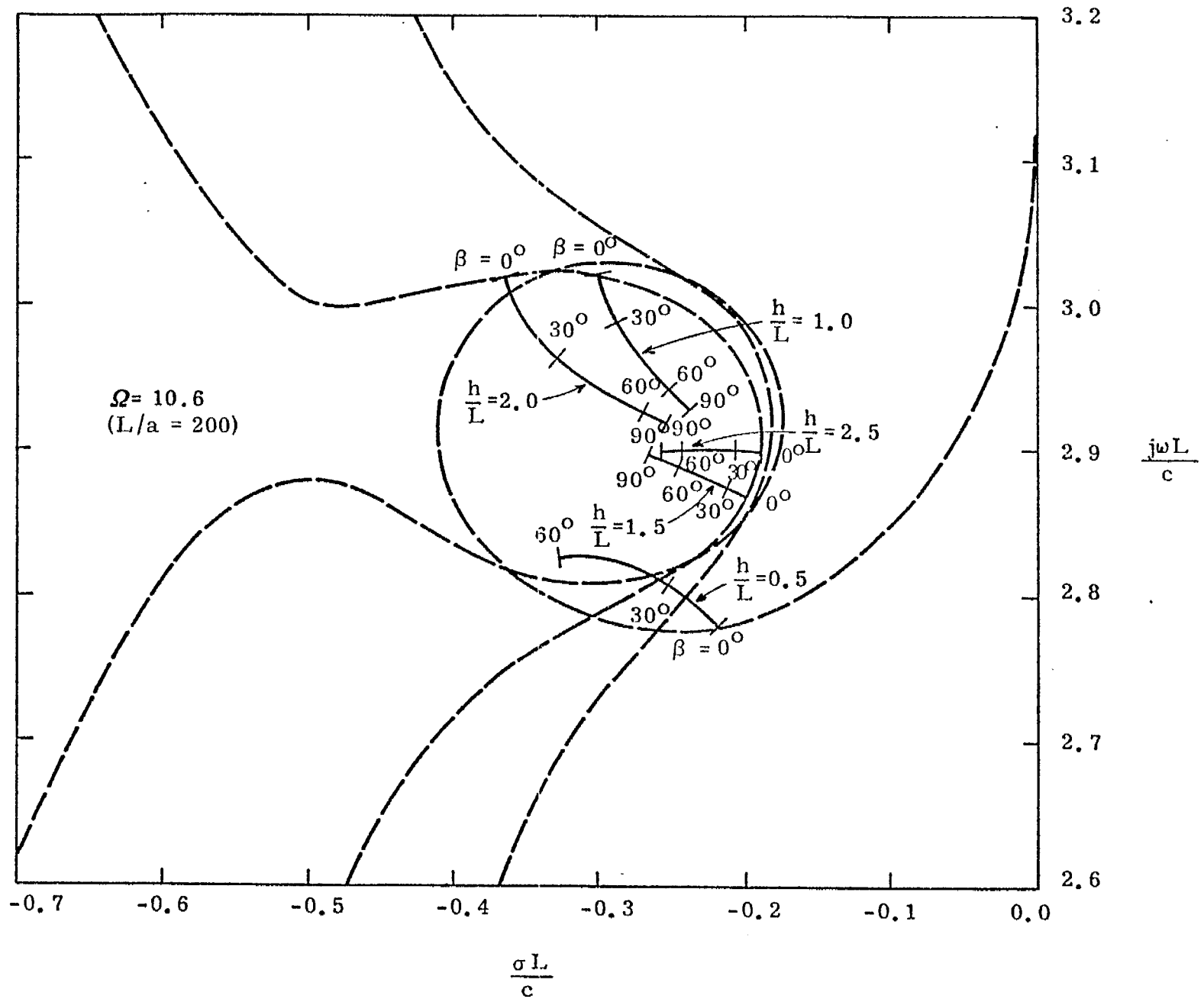
Figure 22. Trajectory of the first scatterer resonance associated with length L as a function of h/L and β.
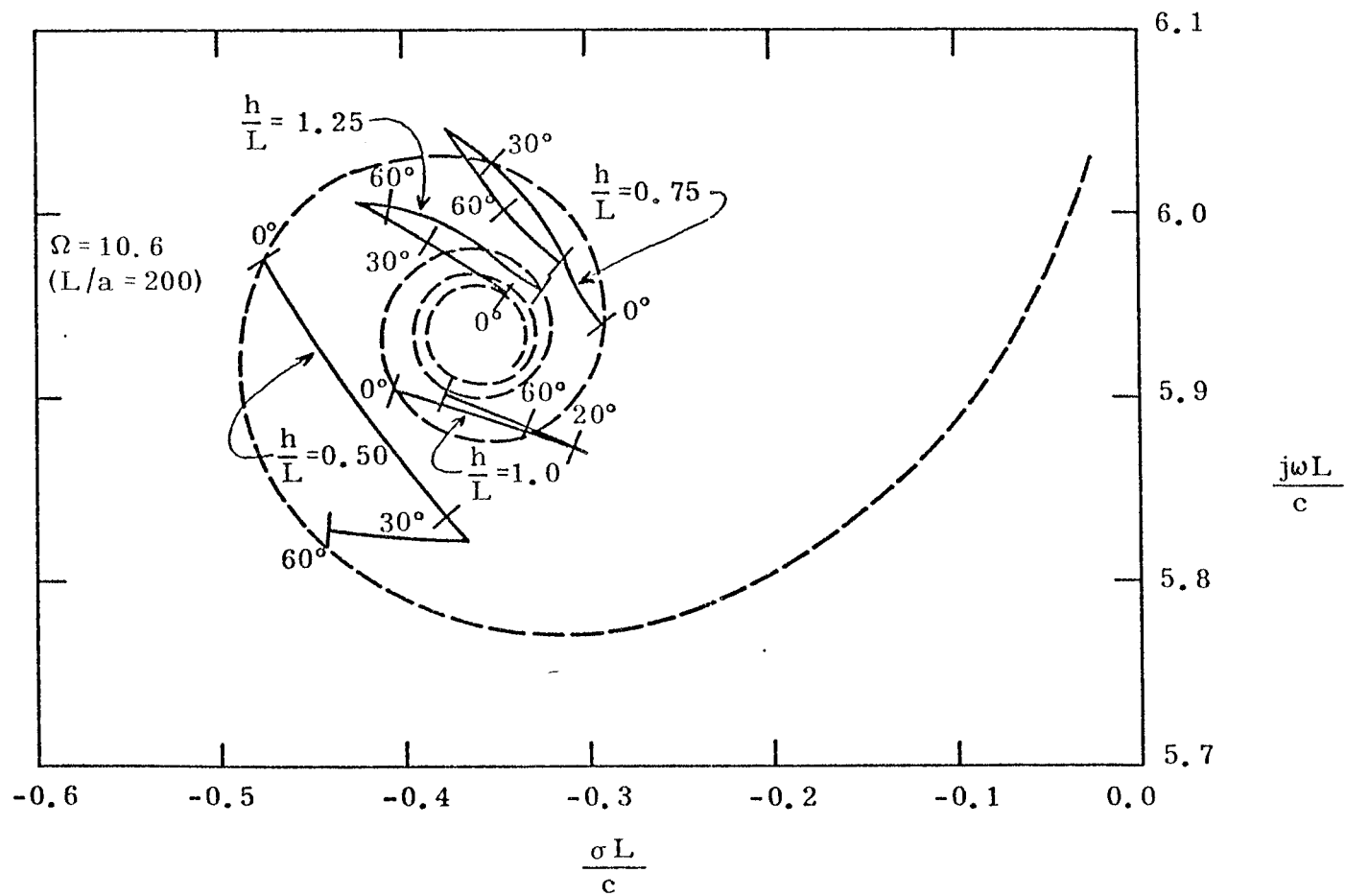
Figure 23. Trajectory of the second scatterer resonance associated with length L as a function of h/L and β.
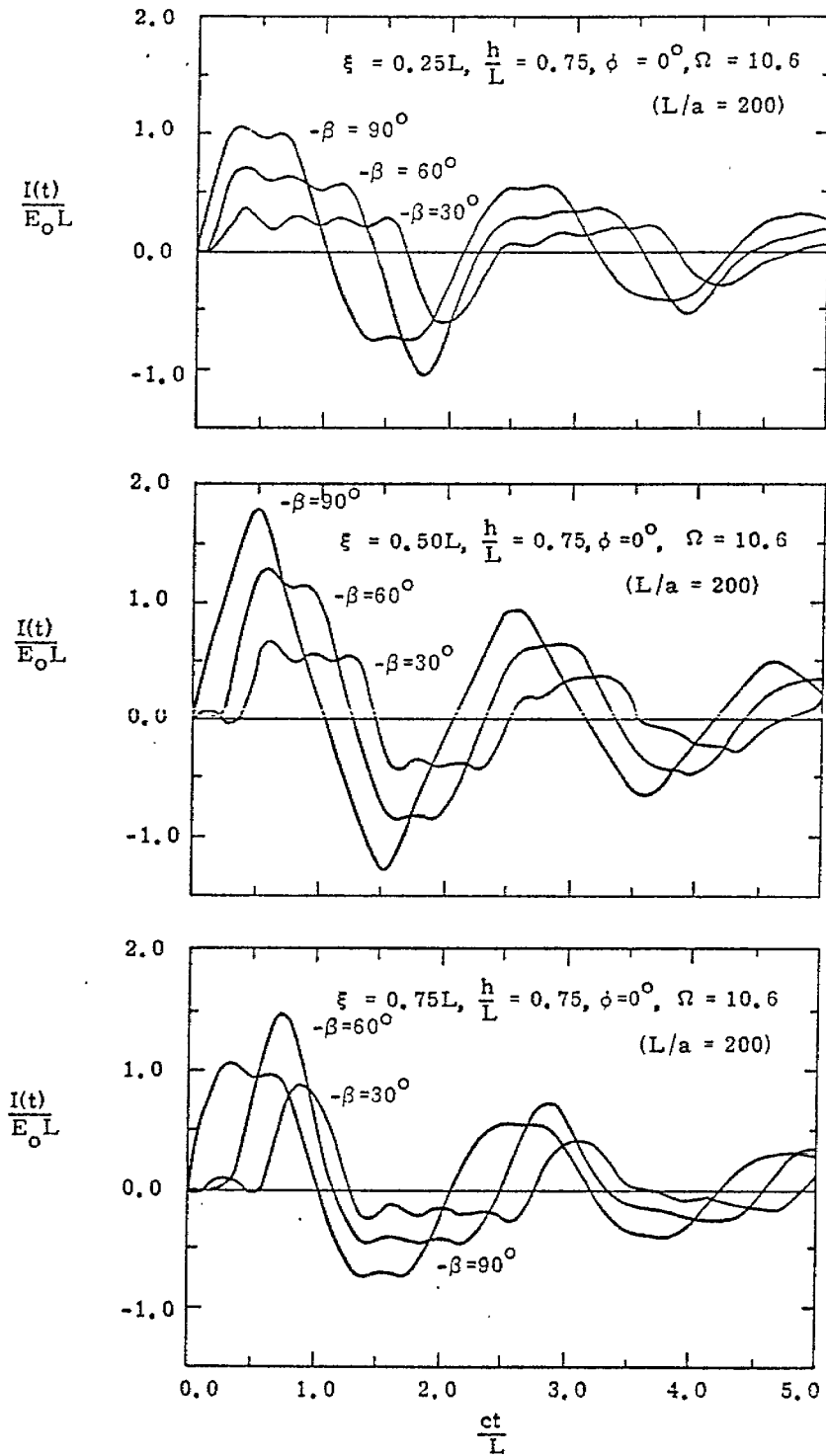
Figure 24.   Time history of the current on the thin-wire
scatterer above the ground. (Results obtained
using contributions from the first five cylinder
singularities nearest the $j\omega$ axis.)
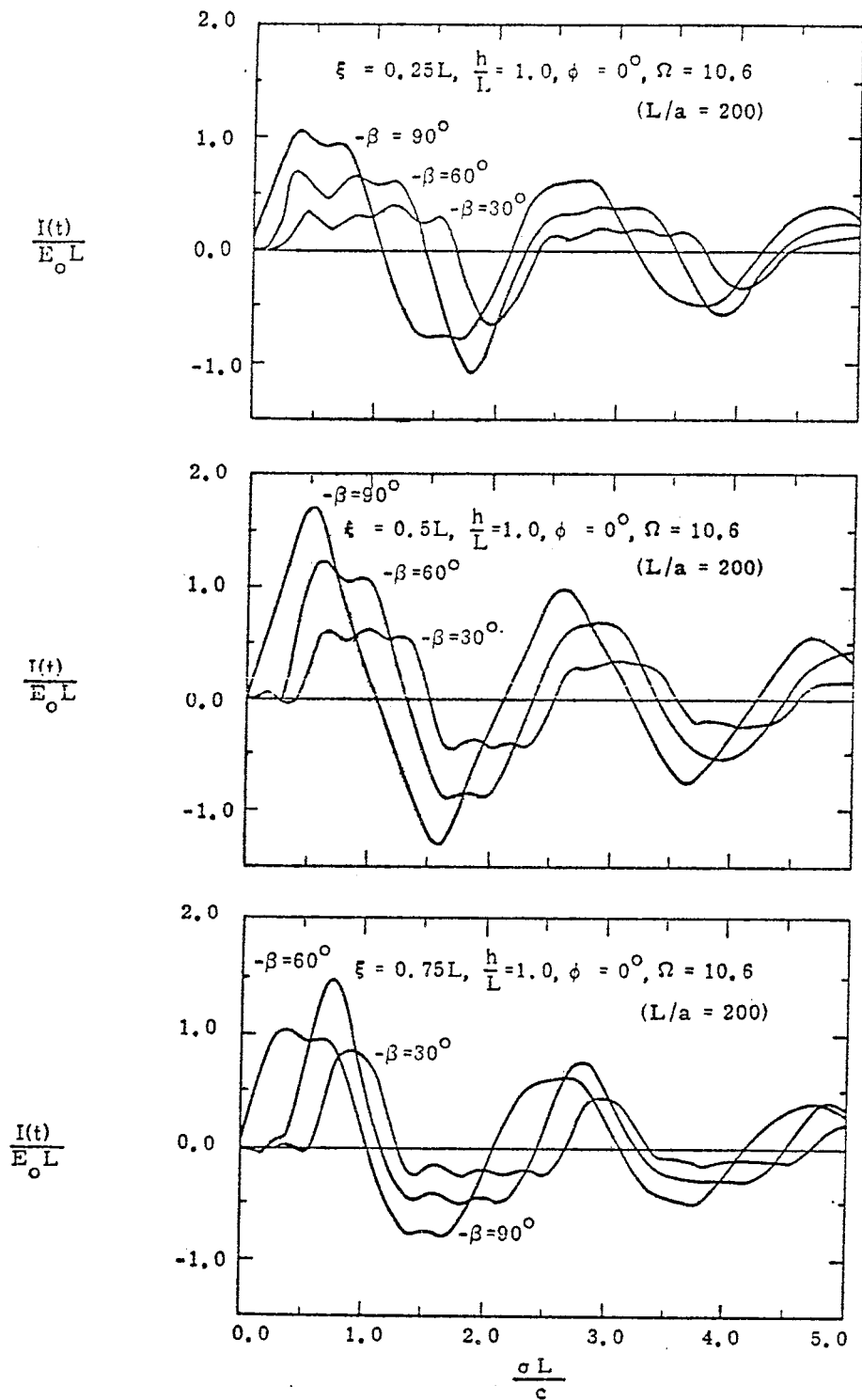
Figure 25. Time history of the current on the thin-wire scatterer above the ground. (Results obtained using contributions from the first five cylinder singularities nearest the $j\omega$ axis.)
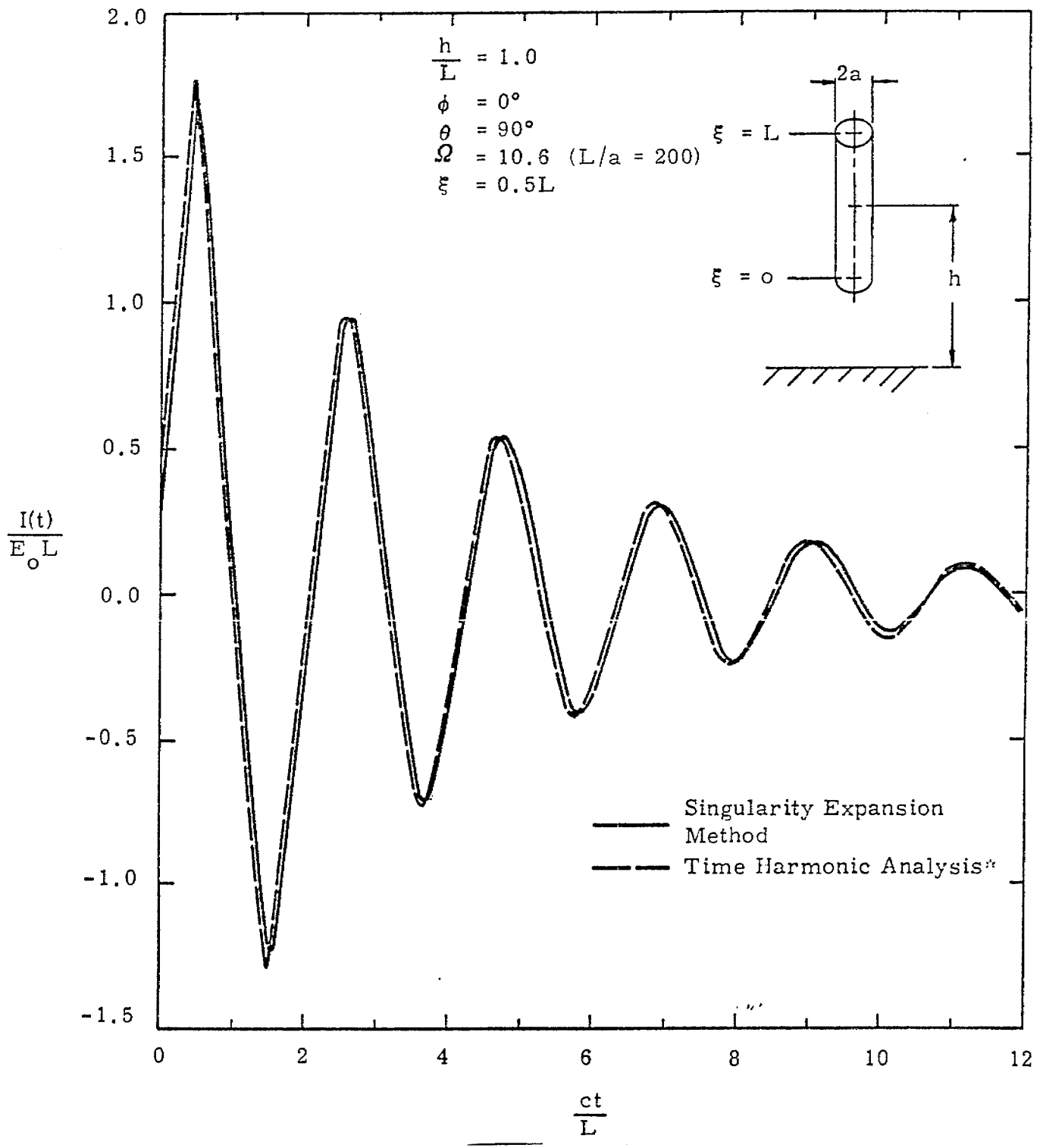
Figure 26. Time history of the current induced on the thin-wire
scatterer above a ground plane (*courtesy of
F. M. Tesche).
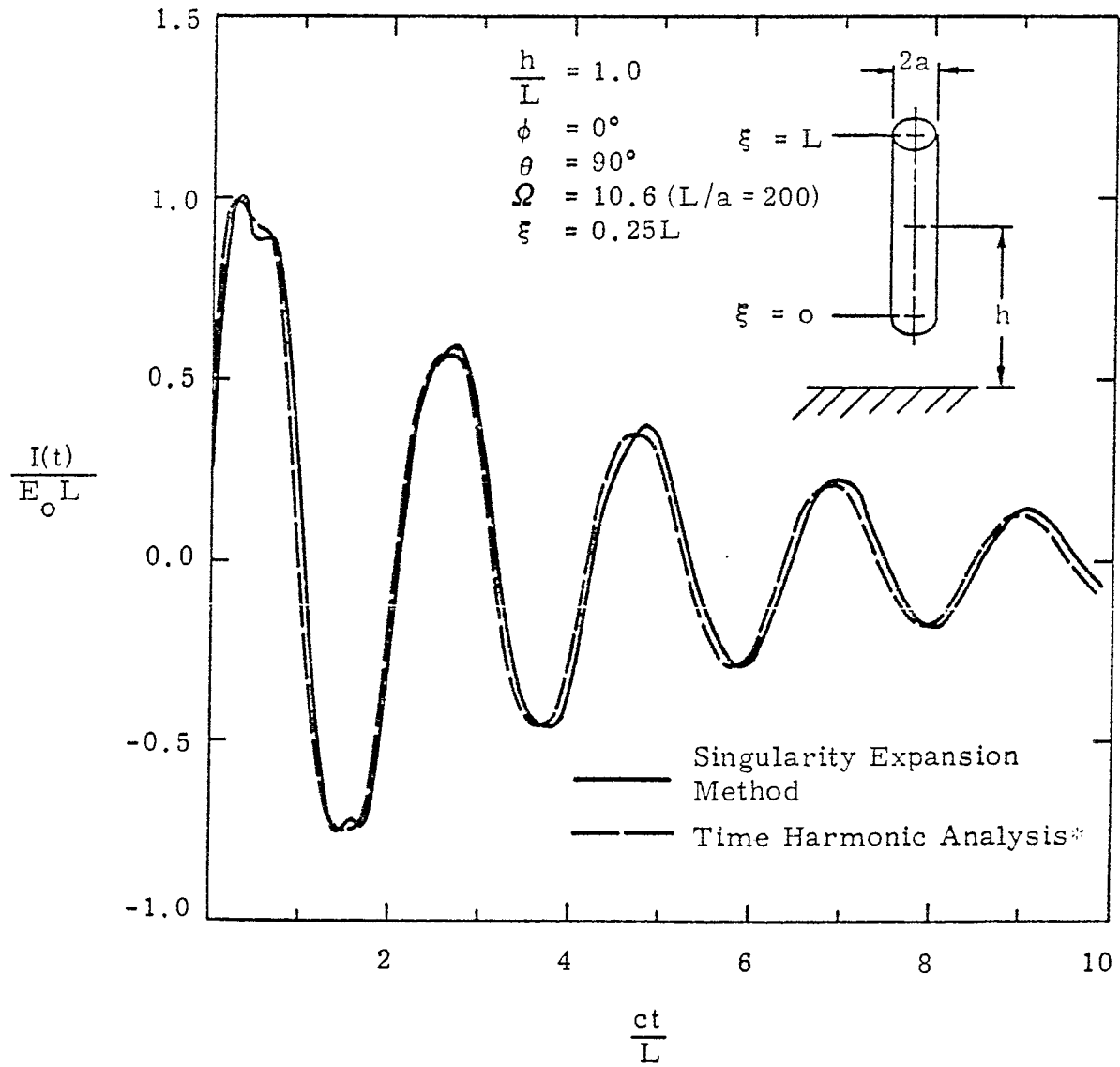
Figure 27.   Time history of the current induced on the thin-wire
             scatterer above a ground plane (*courtesy of
             F. M. Tesche).
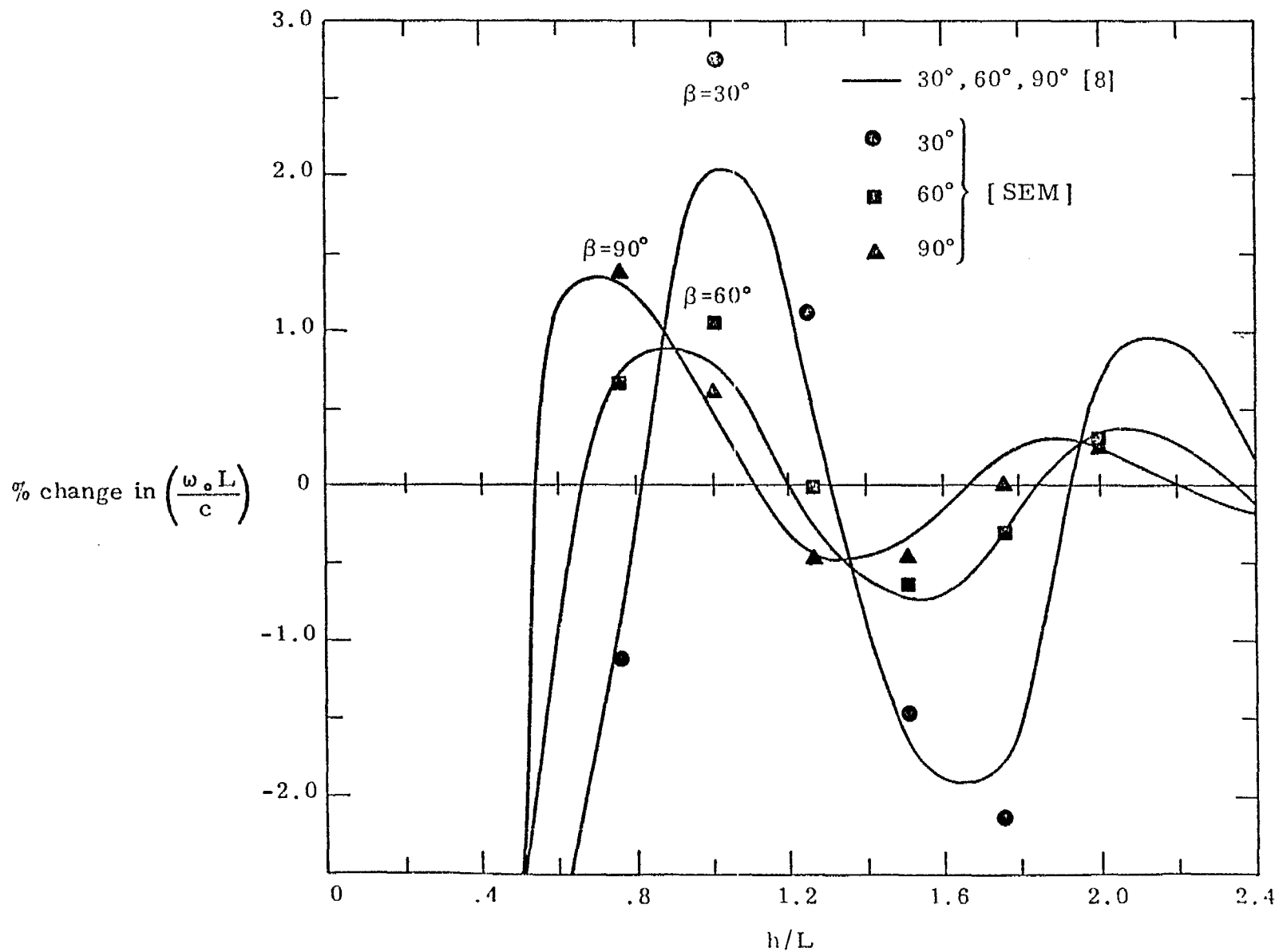
Figure 28. Plots of the percent change of the first resonant frequency of the wire scatterer relative to the free space resonant frequency, shown as a function of h/L for various values of the inclination angle β.

$$\sigma_{fs}[8] = 0.259$$

$$\sigma_{fs}[SEM] = 0.258$$
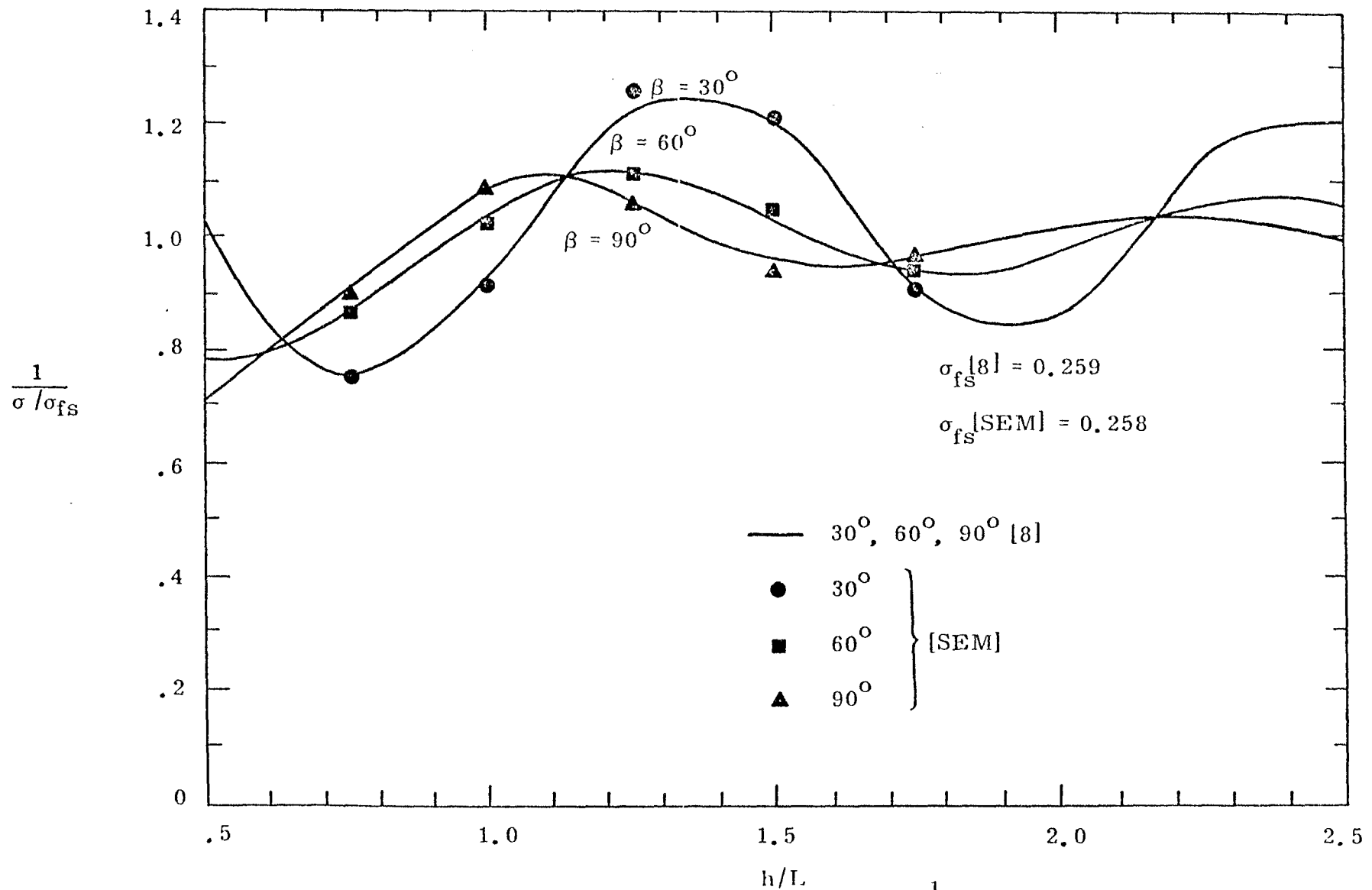
Figure 29. The normalized damping constant $\dfrac{1}{\sigma/\sigma_{fs}}$ for the fundamental mode. Shown as a function of h/L with β as a parameter. The normalizing factor is the damping constant for the fundamental mode of the scatterer in free space.

h/L	[8] $\sigma(90)$	[SEM] $\sigma(90)$
1.0	0.237	0.236
1.5	0.267	0.265
2.0	0.253	0.254
2.5	0.260	0.260
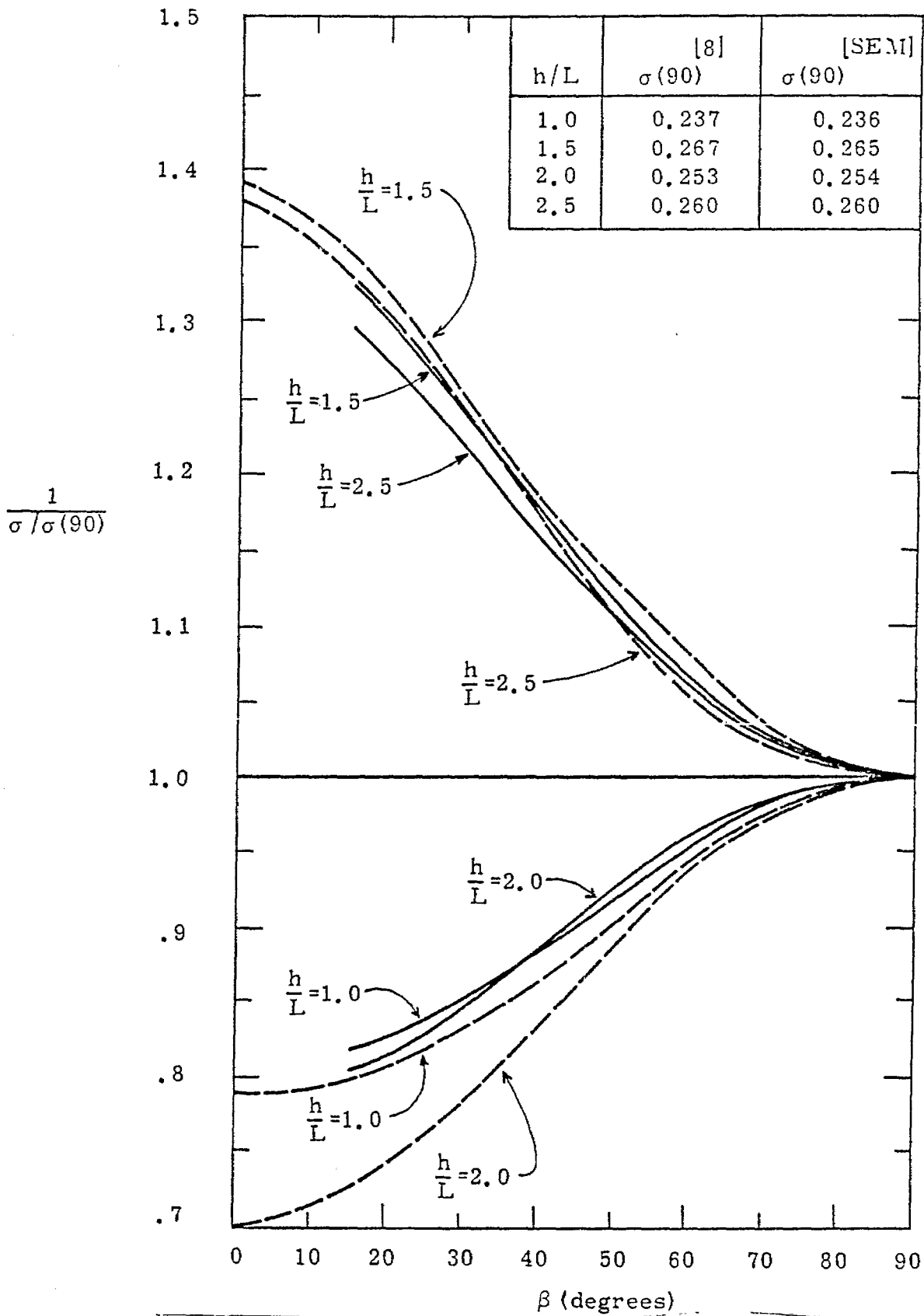
Figure 30. The normalized damping constant $\dfrac{1}{\sigma/\sigma(90)}$ shown as a function of β for h/L as a parameter. The normalization factor $1/\sigma(90)$, is the damping constant calculated for $\beta = 90°$ and the h/L value under consideration.